BOX 1 | CONTINUED

15. Analyze the mass spectrum by fast atom bombardment mass spectrometry (FAB-MS) (m/z) using triethanolamine as the matrix. Confirm the peak at 343 that corresponds to 2-NBDG-H$^+$.
16. Analyze the fluorescent spectrum according to the following steps: (i) Dissolve 2-NBDG with distilled water to adjust the concentration to 10 μg ml^{-1}. (ii) Measure emission spectrum from 495 to 650 nm under excitation at 475 nm. (iii) Measure the fluorescence intensity at 550 nm by scanning the excitation wavelength from 300 to 520 nm. (iv) Typical spectra depicted in **Figure 1d** will be obtained.

- D-Glucose (Wako)
- Cytochalasin B (Sigma, cat. no. C6762)

EQUIPMENT

- 35-mm culture dish with an oval glass bottom (14 × 5 mm^2, 0.08–0.12-mm-thick glass) (Matsunami Glass Ind., Osaka, Japan, cat. no. D110500) (**Fig. 2**) (see EQUIPMENT SETUP)
- Cover glass (cut into 10 × 11 mm^2 pieces) (Corning, cat. no. 1)
- Vacuum grease (HVAC-G; Shin-Etsu Silicone, Tokyo, Japan)
- Round-type, heating glass stage with a flat surface (0.5 mm thick, MPF-10HF) (Kitazato Supply, Fuji, Shizuoka, Japan) or equivalent
- Superfusate warmer (MT-1, dead volume= 0.13 ml; Narishige, Tokyo; or SF-28, Warner)
- Thermistor probe (IT-23, diameter= 0.23 mm; World Precision Instruments)
- Digital thermometer (TH-5; Physitemp Instruments, Clifton, NJ)
- Inverted microscope (Nikon DIAPHOT TMD300 or equivalent) equipped with long working distance (WD) objective lenses: Nikon CF Plan×2 (NA 0.05, WD 5.8 mm), Plan ×4 DL (NA 0.13, WD 16.2 mm), Plan ×10 DL (NA 0.3, WD 9.2 mm) and Plan Fluor ×20 DLL Ph2 (NA 0.5, WD 2.1 mm) or Plan ELWD ×20 DL Ph2 (NA 0.4, WD 7.0–8.1 mm)
- Dichroic mirror (DM), excitation (Ex) and barrier (BA) filters used for 2-NBDG measurement are Nikon DM 505, Ex 480/40 and BA520–560, respectively
- Neutral density (ND) filters: Nikon ND2 (50%), ND4 (25%) and ND8 (12.5%) for fluorescent imaging; ND2 and ND16 (6.25%) for transmitted light imaging; variable intensity is obtained by using these filters in combination
- Peristaltic pump (MCP Standard pump equipped with 12 roller-pumphead MS/CA4-12; Ismatec SA, Glattbrugg, Switzerland)
- Vacuum pump (DAP-15; Alvac, Kanagawa, Japan)
- Vacuum pressure gauge
- Imaging system (Argus 50; Hamamatsu Photonics, Hamamatsu, Japan) or equivalent
- Silicon intensified target (SIT) camera (Hamamatsu Photonics) or equivalent

REAGENT SETUP

CMF-PBS NaCl, 137 g l^{-1}; KCl, 4.0 g l^{-1}; $NaH_2PO_42H_2O$, 0.36 g l^{-1}; KH_2PO_4, 0.18 g l^{-1}; $NaHCO_3$, 12 g l^{-1}; glucose, 11 g l^{-1}; pH 7.30–7.35.

KRB NaCl, 129 mM; KCl, 4.7 mM; KH_2PO_4, 1.2 mM; $CaCl_2$, 1.0 mM; $MgSO_4$, 1.2 mM; $NaHCO_3$, 5.0 mM; HEPES, 10 mM; pH 7.35–7.40.

Preparation of MIN6 cells (i) Prepare a total of 92 ml DMEM-HG containing 13% FBS (FBS-DMEM-HG) in two 50-ml tubes by adding 6 ml FBS to 40 ml DMEM-HG for each tube. (ii) Prepare two 10-cm culture dishes and add 10 ml FBS-DMEM-HG into each dish. (iii) Prepare 15 ml CMF-PBS. (iv) Prepare 1 ml trypsin–EDTA. (v) Warm (i–iv) at 37 °C for the following steps. (vi) Exchange medium in a 10-cm dish culturing MIN6 cells with 10 ml CMF-PBS. (vii) Suck CMF-PBS with a vacuum pump and add 5 ml CMF-PBS and 1 ml 0.25% trypsin–EDTA. (viii) After waiting for 1–2 min, peel off the cells gently by sucking and blowing the medium through a 10-ml pipette. (ix) Suck the cell suspension (approximately 6 ml) and transfer into 30 ml FBS-DMEM-HG. (x) Centrifuge at 1,500 r.p.m. for 3 min (in a Kubota 5200, Kubota Co., Tokyo, Japan). (xi) Suck the supernatant and add 10 ml FBS-DMEM-HG. (xii) Triturate five times with a 10-ml pipette (let cells go back and forth gently within the pipette using a Pipette aid). (xiii) Centrifuge at 1,500 r.p.m. for 1 min (in a Kubota 5200, Kubota Co., Tokyo, Japan). (xiv) Add 3 ml FBS-DMEM-HG. (xv) Triturate 40 times with a 5-ml pipette, and count cells within 30 s. (xvi) Dilute cell suspension at 20 × 10^4 ml^{-1}. (xvii) For passage, transfer 0.5 ml cell suspension into each of the 10-cm dishes containing 10 ml FBS-DMEM-HG (ii). (xviii) For the experiment, triturate 20 times again and transfer cell suspension (145 μl) onto the glass part of a glass-bottom culture dish. Moisten the glass part of the dish with 100 μl FBS-DMEM-HG beforehand and suck medium just before plating. (xix) Observe cells after waiting for 5 min and readjust the dilution ratio so that most cells are seen separately. If too many cells are observed, blow off cells with yellow tip and dilute again. (xx) Leave the cells in a CO_2 incubator (5% CO_2, 37 °C) for 30 min until the cells adhere to the glass. (xxi) Add 2 ml FBS-DMEM-HG to fill the whole culture dish. (xxii) Perform measurement of 2-NBDG uptake before many clusters of MIN6 cells are formed. To assess the health of MIN6 cells during the course of the passages, check [Ca^{2+}] responsiveness to glucose stimulation similarly to the procedure described in **Box 2** (**Figs. 2** and **3**).

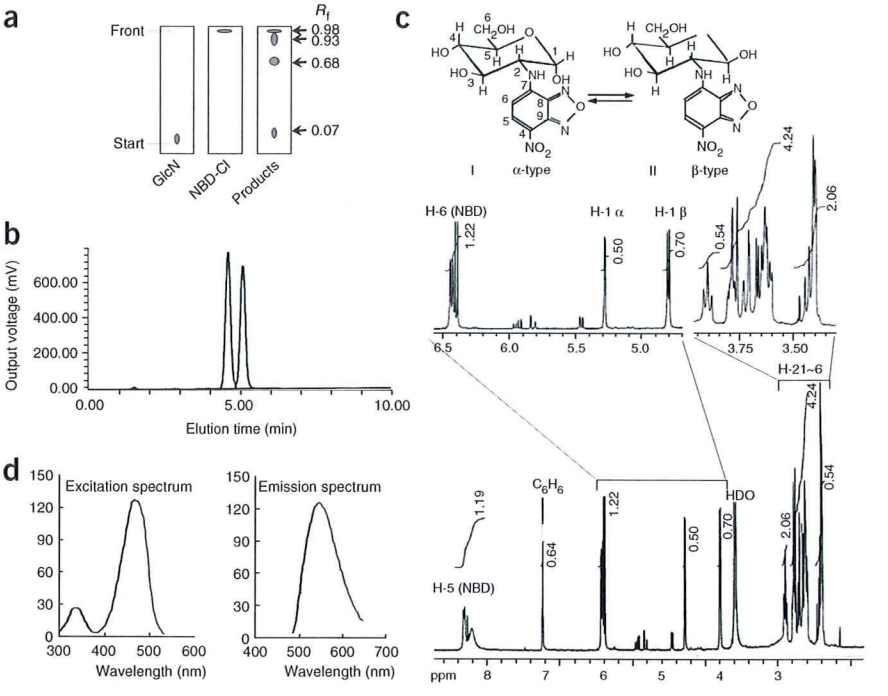

Figure 1 | Analytical data of 2-[*N*-(7-nitrobenz-2-oxa-1,3-diazol-4-yl)amino]-2-deoxyD-glucose (2-NBDG). (**a**) TLC. Silica gel plate, solvent CH_3CN:H_2O = 17:3, R_f (fluorescent spots: 2NBDG = 0.68, NBD-Cl = 0.98, GlcN = 0.07, unidentified by-products = 0.93). (**b**) HPLC spectrum. Column: TSKgel amide-80, eluent: CH_3CN:H_2O = 17:3, flow rate: 1.0 ml min^{-1}, detection: $OD_{475\ nm}$. Two peaks: α-D-anomer and β-D-anomer. (**c**) ^{1}H-NMR spectrum. 500 MHz in D_2O, δ4.78 p.p.m. (d, $J_{1,2}$ = 10 c.p.s., axial–axial, β), δ5.27 p.p.m. (d, $J_{1,2}$ = 4 c.p.s., axial–equatorial, α), δ3.4–3.95 p.p.m. (m, H-2–H-6), δ6.4 p.p.m. (*m*, H-6 NBD), δ8.2–8.35 p.p.m. (*m*, H-5 NBD). (**d**) Fluorescence spectra. Emission spectrum: λ_{EM} = 495–650 nm, λ_{EX} = 475 nm; excitation spectrum: λ_{EM} = 550 nm, λ_{EX} = 300–520 nm.

Preparation of 2-NBDG solution Dissolve 2-NBDG in KRB (pH 7.35–7.40). The concentration of 2-NBDG and glucose should be determined according to the purpose of the experiment (see PROCEDURE). ▲ CRITICAL Do not freeze the 2-NBDG solution, as it will precipitate when thawing.

EQUIPMENT SETUP

Culture dish and superfusion chamber Mark random scratches beforehand on the outside of the oval glass bottom of the culture dish with a diamond knife for later immunocytochemical identification of the cells. Although a round glass-bottom culture dish can be used, the medium flow is smoother in an oval one. Prepare a plastic plate with a leaf-shaped hole, as the glass part of the dish is too shallow to obtain a stable medium flow (**Fig. 2**). This plate can be readily made using the culture dish by removing its glass bottom. Attach the plate tightly to the plastic part of the culture dish with vacuum grease just before experiment (see PROCEDURE). Thus, the depth of the glass part of the dish is doubled. A silicone rubber plate with an oval hole can be used instead of the plastic plate (**Fig. 2**). In this case, small projection portions made on the silicone plate (slashed part in **Fig. 2**) will help precise positioning of the cover glass.

Attach a square small cover glass (10× 11 mm^2) to the plastic plate with a small amount of vacuum grease to cover the central part of the oval glass bottom (**Fig. 2**). The cover glass helps to smooth flow while decreasing the volume of superfusate, assuring rapid change of the solution, and also helps to prevent optical noise owing to fluctuation of the medium surface level. When only the central part of the bath is covered, drugs can be directly dropped onto the small gap upstream of the cover glass. In addition, local temperature at the region of interest below the cover glass can be easily checked during the experiment. ▲ CRITICAL Adjust the position, angle and height of the inlet and, especially, the outlet needle carefully **Fig. 2**) to obtain smooth laminar flow.

Place a round, flat-surface heating glass stage on the microscope stage. A plastic holder plate (14 × 14 × 0.9 cm^3) with an opening (approximately 35 mm) in the central part should be fixed on the heating stage. The inner diameter of the opening must be determined by the outer diameter (sometimes tapered) of the dish used. Mount the culture dish into the plastic holder plate so that the glass bottom of the culture dish directly touches the heating glass stage (37 °C). Long-WD objective lenses (see EQUIPMENT) are required owing to the thickness of the heating glass stage.

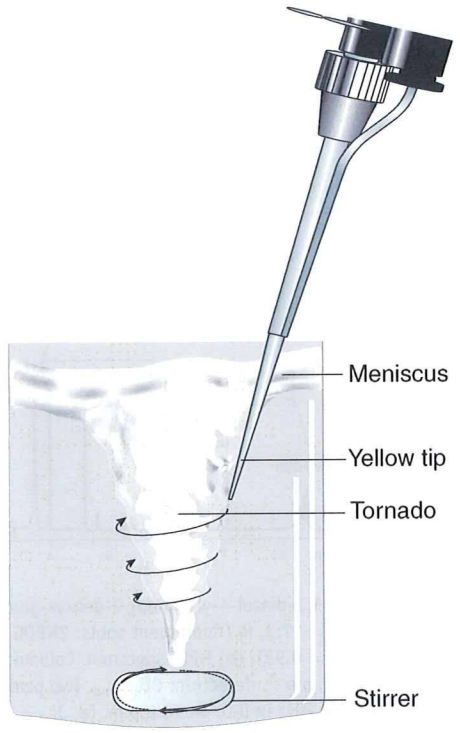

Figure 3 | Dissolving fura-2/AM in DMSO into Krebs Ringer bicarbonate buffer (KRB).

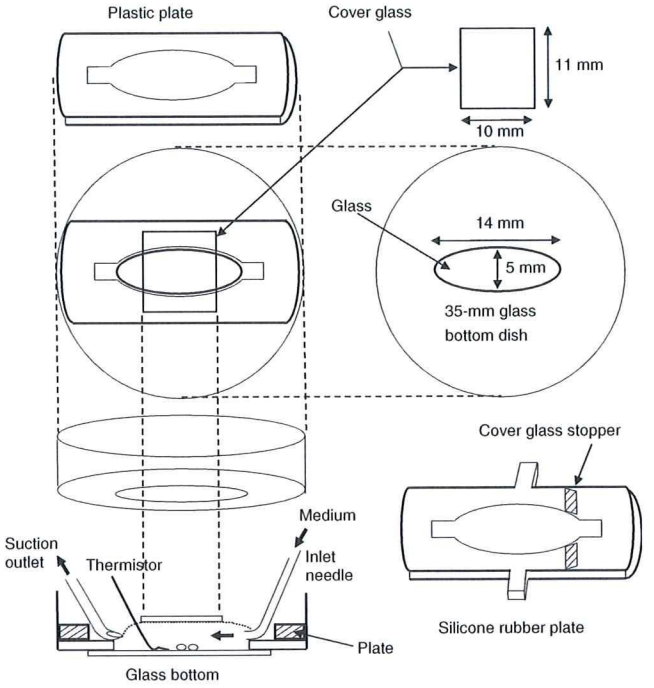

Figure 2 | A culture dish–based chamber for live-cell imaging. A plastic (or silicone rubber) plate is attached to the glass-bottom culture dish to make a bath for superfusion. The central part of the bath is covered by a cover glass to promote smooth flow and rapid exchange of superfusate.

Check the temperature of the superfusate at the region of interest by inserting a very thin thermistor probe between the cover glass and the glass bottom before (or sometimes during) the experiment. An extra dish with no cells should be prepared for just this purpose. Constant temperature at the area of interest (36.5–37.5 °C) indicates that the whole chamber system is working properly.

Use a low-pulsation peristaltic pump and a vacuum pump for the delivery and the removal of the superfusate, respectively. Substitution of the polyethylene tube with a stainless steel pipe of very thin internal diameter helps to decrease dead volume from the superfusate bottle to the dish. Adjust the vacuum pressure with a screw valve and/or three-way valves at 30–40 kPa so that cells are left on the dish. A simple delivery system using hydrostatic pressure can be used instead of a peristaltic pump. ▲ CRITICAL The shape of the end of the outlet needle for removing superfusate is critical to achieving a stable flow. The main consideration is that the hole at the end should be opened in the upward direction (**Fig. 2**). Bend a stainless steel needle (20G, 0.90 × 70 mm) smoothly so as not to interfere with smooth medium flow inside the needle. Then enlarge the hole at the end of the needle obliquely to the axis as large as is possible using sandpaper so that the needle has an elongated hole on the very tip. When the position and the angle of the needle are adequate, superfusate is sucked constantly from the hole together with air, making a constant sucking sound. We have designed a height-, angle- and rotation-adjustable small holder for the needle for this purpose (**Fig. 4**); this is available from Narishige Scientific Instruments, Tokyo, Japan (see **Table 1**).

PROCEDURE

Preparation for superfusion ● TIMING 5 min

1| Take the culture dish out from the CO_2 incubator, and gently absorb the culture medium outside the glass bottom part of the dish. Then wipe the medium left on the plastic floor of the dish completely using a cotton swab, leaving medium only on the glass bottom part.

2| Attach the plastic plate with a leaf-shaped hole (**Fig. 2**) tightly to the culture dish with silicone vacuum grease.

BOX 2 | $[Ca^{2+}]_I$ MEASUREMENT COMBINED WITH MEASUREMENT OF 2-[*N*-(7-NITROBENZ-2-OXA-1,3-DIAZOL-4-YL)AMINO]-2-DEOXY-D-GLUCOSE (2-NBDG) UPTAKE IN PANCREATIC ISLET CELLS

REAGENTS

- Fura-2/AM (Dojindo, cat. no. 343-05401)
- DMSO (Dojindo)
- Ca^{2+}-free Krebs Ringer bicarbonate buffer (KRB) (see REAGENT SETUP below)
- $CaCl_2$ (0.1 M solution) (Wako)
- Glucose (Wako)
- Eagle's minimum essential medium containing kanamycin (60μg ml^{-1}) (Nissui, cat. no. 1) and 5.6 mM glucose (MEM)
- EGTA (0.1 M solution) (Sigma, cat. no. E-4378)
- BSA (Fraction V, pH of 1% aqueous solution is 5.2) (Sigma, cat. no. A-4503)
- Tolbutamide (Sigma, cat. no. T0891)
- Guinea pig anti-swine insulin antibody (Dako, cat. no. N1542)
- Rabbit anti-porcine glucagon antibody (Dako, cat. no. L1813)
- Rhodamine-conjugated goat anti-rabbit IgG (Cappel)
- Rhodamine-conjugated goat anti-guinea pig IgG (Chemicon)
- Sodium phosphate buffer (PB)
- Paraformaldehyde (Nakalai)

EQUIPMENT

- Non-coated glass-bottom dishes
- Dichroic mirror and barrier filter (Nikon DM400) (BA510 LP)
- Excitation filter Hamamatsu MC340- and 380-nm excitation filters

REAGENT SETUP

Preparation of islet cells (i) Isolate islets of Langerhans from 8–12-week-old Harlan Sprague–Dawley rats by collagenase digestion under nembutal anesthesia[25]. (ii) Transfer the islets into ice-cold Ca^{2+}-free KRB containing 5.6 mM glucose. (iii) Centrifuge at 800 r.p.m. for 30–60 s (in a himac CR5B from Hitachi High Technologies, Tokyo, Japan) at room temperature (22–28°C) and wash sediments with KRB containing 0.1 mM Ca^{2+}, 0.1% BSA and 5.6 mM glucose (repeat three times). A small addition of Ca^{2+} at this point will mitigate cellular damage by EGTA treatment in the next stage. (iv) Dissociate the islet into single cells by incubation for 15–17 min at room temperature in 200μl Ca^{2+}-free KRB containing 1 mM EGTA, 0.1% BSA and 5.6 mM glucose. Make a 0.1 M EGTA stock solution for this purpose (adjust pH to 7.4 by 1 N HCl). (v) Triturate 8–12 times using a yellow tip. (vi) Transfer the dissociated islets into 10 ml of MEM supplemented with 10% FBS (MEM-FK). (vii) Centrifuge at 800 r.p.m. for 3 min (in a himac CR5B from Hitachi High Technologies, Tokyo, Japan) at room temperature, discard the supernatant by suction pipette and re-suspend the cells in 200μl of MEM-FK. (viii) Plate a small amount of single cells (such as 30μl) on a culture dish in the center of the oval glass bottom (**Fig. 2**). (ix) Leave the cells in a CO_2 incubator (5% CO_2, 37 °C) for 20 min until cells adhere to the glass bottom. (x) Add 0.5–1.0 ml of culture medium slowly. Cells can be maintained in the CO_2 incubator for up to 2 d. However, Ca^{2+} responsiveness to glucose stimulation is obtained from a maximal number of healthy β-cells during the several hours after plating.

Ca^{2+}-free KRB (mM) NaCl, 129; KCl, 4.7; KH_2PO_4, 1.2; $MgSO_4$, 1.2; $NaHCO_3$, 5.0; HEPES, 10; pH 7.35.

Preparation of fura-2/AM solution

1. Dissolve 10 μl 1 mM fura-2/AM in DMSO solution into 10 ml KRB containing 2.8 mM glucose and 1 mM Ca^{2+} (final concentration of fura-2/AM, 1 μM), as described.

Note: Use DMSO that has been kept dried, since moisture absorption interferes with dissolution of fura-2/AM (in DMSO) into aqueous solution. Detergents to promote dissolution such as Cremophor EL (C5135, Sigma) are not necessary. The volume of fura-2/AM-containing KRB should be determined according to the chamber volume and the total dead volume in the inlet tubing.

2. Stir vigorously 10 ml KRB solution in a small glass vial (such as 12.5 ml) using a very small stirrer magnet so that a stable, tornado-like vortex appears in the central part of the solution (**Fig. 3**). Use a high-performance magnetic stirrer.

Note: If a low-performance stirrer is used, the position of the vortex may move right or left unstably, and dissolution will be unsuccessful.

3. Push out the fura-2/DMSO solution continuously and as slowly as possible from a yellow tip. Hold the tip almost perpendicularly along, but slightly outside, the vortex wall. When dissolution is successful, fura-2/AM in DMSO disappears spirally into the KRB solution similar to a pale smoke or is almost unseen. Never suck the KRB into the tip by releasing pushing force.

Note: If water leaks into the tip, small oil droplets will be seen coming out from the tip into the KRB when fura-2/AM is pushed out, and the tip end will be polluted by white deposit. These droplets are due to undissolved fura-2, indicating unsuccessful dissolution. Discard the tip and try again from the beginning in such a case.

4. When subdivided into aliquots, keep fura-2/AM at below −20 °C in a tightly sealed box containing hygroscopic material to prevent moisture absorption during frequent use.

Preparation of glucose responsiveness experiment

1. Make KRB containing 1 mM Ca^{2+} as a superfusate during measurement. Make 100 ml of 0.1 M $CaCl_2$ stock solution to add Ca^{2+} to KRB. Prepare KRB containing 2.8 and 16.8 mM glucose.
2. Adjust pH of KRB stock solution to 7.3 with NaOH, because it will shift to 7.35–7.40 by the day of experiment.

Note: pH exceeding 7.4 may produce unsuccessful results.

BOX 2 | CONTINUED

3. Prepare tolbutamide in KRB by dissolving 1 M stock solution of tolbutamide (in DMSO) into KRB containing 2.8 mM glucose in a manner similar to that depicted in **Figure 3** (final concentration of tolbutamide, 200μM).

PROCEDURE

Measurement of $[Ca^{2+}]_i$ in response to glucose stimulation: *fura-2/AM loading* ● TIMING **30 min**

1. Prepare 10 ml of KRB (depending upon the total dead volume in the inlet tubing) containing 2.8 mM glucose and 1μM fura-2/AM for each culture dish.
2. Superfuse the islet cells with the fura-2/AM in KRB at a flow rate of 0.3 ml min^{-1} for 30 min at 37 °C.
3. Wash fura-2/AM solution with KRB containing 2.8 mM glucose at 37°C. This protocol is both easy and time saving. Indeed, because only islet cells strongly adhered to the glass bottom are left on the dish after the loading, cells of interest can be searched for using the microscope immediately after fura-2/AM loading, which contributes to obtaining responses from cells still in a healthy condition.
4. As an alternative to the above method of loading fura-2/AM by superfusion, fura-2/AM can be loaded by exchanging culture medium with KRB containing 2.8 mM glucose and 1 μM fura-2/AM, and incubated for 30 min at 37 °C in a humidified atmosphere containing 5% CO_2 (in a CO_2 incubator).

Measurement of $[Ca^{2+}]_i$ in response to glucose stimulation: $[Ca^{2+}]_i$ measurement ● TIMING **1 h**

5. Superfuse KRB containing 2.8 mM glucose. Start searching the area of interest without waiting additional post-loading minutes for the hydrolysis of AM residue, as the searching process is usually time consuming.
6. Capture transmitted light images of cells of interest.
7. Start imaging the ratio F340/F380. Fura-2 fluorescence is detected every 5 or 10 s at 500–520-nm wavelength following excitation at 340-nm (F340) and 380-nm (F380) wavelengths. The ratio image is obtained using an Argus 50. (See Troubleshooting section below.)
8. Exchange superfusate to KRB containing 16.8 mM glucose for 5–10 min and then return to KRB containing 2.8 mM glucose.
9. After the ratio recovers to baseline for about 10 min or so, check responsiveness of β-cells to tolbutamide by superfusing KRB containing 200 μM tolbutamide for a brief period within 30 s.

Measurement of 2-NBDG uptake ● TIMING **30–60 min**

10. After finishing Ca^{2+} imaging, start measurement of 2-NBDG uptake in a manner similar to that described for MIN6 cells. To discriminate β-cells from other cell types, KRB containing 200μM 2-NBDG and 2.8 mM glucose is loaded for 1 min. Quenching of fura-2 fluorescence is not required since the 2-NBDG fluorescence is strong enough in comparison with fura-2 fluorescence, and the 2-NBDG uptake is evaluated by the relative increase in the fluorescence.

ANTICIPATED RESULTS

A raw example of measurement of $[Ca^{2+}]_i$ and subsequent 2-NBDG uptake in pancreatic islet cells is shown in **Figure 6**. After loading fura-2/AM by superfusion, a region of interest is selected and a transmitted light image is captured (**Fig. 6a**). Cells to be monitored are then selected on the fluorescent image (**Fig. 6b**). Information on the $[Ca^{2+}]_i$ response to glucose stimulation (**Fig. 6c**) and the subsequent uptake of 2-NBDG by a brief superfusion (**Fig. 6d,e**) were used to evaluate the divergent uptake of heterogeneous islet cells in combination with later immunocytochemistry (**Fig. 6f**). Since islet cells consist of a heterogeneous population of cells, including glucose-responsive insulin-secreting β-cells and glucose-unresponsive glucagon-secreting α-cells as well as somatostatin-secreting δ-cells, later immunocytochemical identification of cell type is essential (see **Box 3**).

TROUBLESHOOTING

Problem: Extraordinary large ratio in $[Ca^{2+}]_i$ imaging.

Possible reason: Unhealthy cells may show a large ratio. Especially important, islet cells do not remain healthy for many hours in KRB containing 2.8 mM glucose. In addition, care should be taken to prevent high-temperature degradation of the coating materials of the emission filter, which can be continuously exposed to heat radiation from the xenon lamp during the experiment despite the heat-insulating lens.

Solution: Carry out experiments using freshly prepared cells. To retard degradation of the coating materials of the filter, empty the home filter position and use two heat-insulating lenses in the pathway from the lamp. The condition of the filters should be checked by making a calibration curve for $[Ca^{2+}]_i$.

▲ CRITICAL STEP A toothpick and a small bent spatula can be used to spread the grease and press the plate, respectively. If you use too much grease, it comes out from the gap between the dish and the plate and interferes with medium flow. If you use too little, the superfusate leaking into the gap will interfere with smooth exchange of the superfusate during drug application, which is especially problematic when high concentrations of 2-NBDG are applied.

3| Cover the central part of the oval glass bottom with a square cover glass with a small amount of vacuum grease (**Fig. 2**).

4| Mount the dish on the plastic holder on the inverted microscope stage and start superfusion immediately with KRB containing 5.6 mM glucose. Paint a small mark on the rim of the dish so that it coincides with the mark on the holder. This makes it possible to reproduce the angle of the dish when immunocytochemistry is conducted later.

BOX 3 | IMMUNOCYTOCHEMICAL IDENTIFICATION OF ISLET CELLS AFTER MEASUREMENT OF 2-[*N*-(7-NITROBENZ-2-OXA-1,3-DIAZOL-4-YL)AMINO]-2-DEOXY-D-GLUCOSE (2-NBDG) UPTAKE

REAGENTS

- Guinea pig anti-swine insulin antibody (Dako, cat. no. N1542)
- Rabbit anti-pig glucagon antibody (Dako, cat. no. L1813)
- Rhodamine-conjugated goat anti-guinea pig IgG (Chemicon)
- Rhodamine-conjugated goat anti-rabbit IgG (Cappel)
- Sodium phosphate buffer (PB)
- Paraformaldehyde (Nakalai)

EQUIPMENT

- Dichroic mirrors and filters: Nikon DM575 (EX 510–560, BA 590 LP)

Immunocytochemistry ● TIMING **5 h–4.5 d**

1. At the end of the measurement of 2-NBDG uptake, capture transmitted light images of the analyzed cells at ×20, ×10, ×4 and ×2 for immunocytochemical identification of their location. Low-magnification lenses are especially convenient for finding the analyzed region in reference to the scratches previously made under the glass bottom of the culture dish.
2. Fix cells in cold 0.1 M PB containing 2% paraformaldehyde overnight at 4°C. Alternatively, pour the cold fixative on the cells and leave cells for up to 1 h at room temperature.
3. Wash three times (rotate the dish gently and wait for 5 min between each washing) with 0.01 M PBS. Cells may be treated with 1% BSA.
4. React cells with primary antibodies, such as guinea pig anti-pig insulin antibody (1:100) or rabbit anti-pig glucagon antibody (prediluted), at room temperature for 1 h or at 4 °C overnight.

Note: Can be left up to 3 d at 4 °C.

5. React with rhodamine-conjugated secondary antibody (1:100–1:500) at room temperature for 1 h.
6. Wash three times with PBS.
7. Mount the dish on the plastic holder on the microscope stage so that the mark on the rim of the dish coincides with the mark on the holder.
8. Show the previous low-magnification image of the cells on the PC monitor and affix tiny triangles made of opaque tape on both ends of individual major scratches observed on the monitor screen. Then find the same scratch pattern by microscope and adjust the field of view so that the identical pattern is seen on the monitor using the opaque triangles as guides. Finer adjustment can be made by comparing the current image with the previous image. Repeat the process in higher-magnification views.
9. Examine rhodamine fluorescence.

ANTICIPATED RESULTS

See **Figure 6f**.

Measurement of 2-NBDG uptake ● TIMING **30–60 min**

5| Select area of interest and capture a transmitted light image.

6| Demarcate cells. Select an area for evaluating changes in background fluorescence.

7| Adjust the gain of the detection system and capture fluorescent images. A transmitted light image with no ND filter is useful for identifying locations of cells on the monitor screen by the intrinsic fluorescence of the cells. Strong ND filters are used when the fluorescence of cells is saturated after loading 2-NBDG.

8| Superfuse MIN6 cells with glucose-free KRB for 15 min.

9| Change superfusate to D-glucose-free KRB containing 50–600 μM 2-NBDG for 15–120 s, and then wash.

▲ CRITICAL STEP The concentration of 2-NBDG and the loading period are to be determined according to the purpose of the experiment, the type of GLUTs of interest and the signal-to-noise ratio of the detection system. For the signal-to-noise ratio and the superfusion technique used in the present system, the shortest practical loading period is 15 s, and the smallest concentration is 50 μM. When 600 μM 2-NBDG is used, a loading period longer than 120 s should be avoided because of the nonlinear increase in the 2-NBDG fluorescence over time[9]. With a system requiring a long loading period (e.g., tens of minutes),

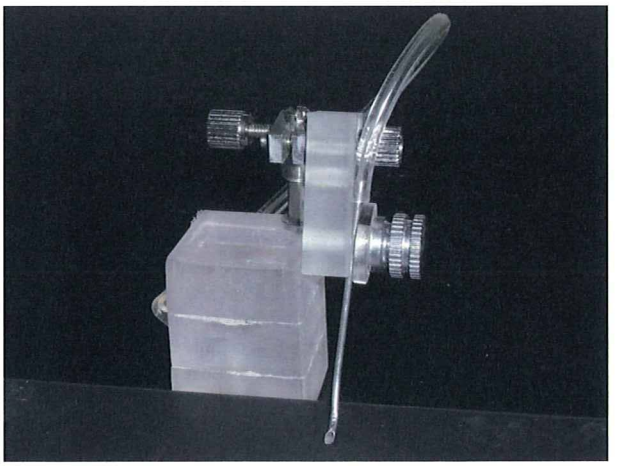

Figure 4 | A custom-made holder for the outlet needle (Narishige). Height, rotation angle and lean angle of the needle are freely adjustable without using a screwdriver.

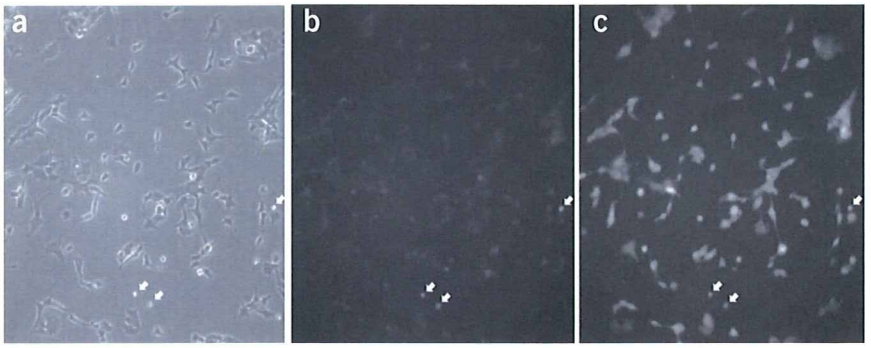

Figure 5 | Measurement of 2-[*N*-(7-nitrobenz-2-oxa-1,3-diazol-4-yl)amino]-2-deoxy-D-glucose (2-NBDG) uptake into MIN6 cells. (**a**) Transmitted light image (×20). Arrows indicate debris of dead cells. Raw fluorescent images measured at 540-nm wavelength with no neutral density (ND) filter (**b**) before and (**c**) after loading Krebs Ringer bicarbonate buffer (KRB) containing 600 μM 2-NBDG for 15 s. Note that no increase in the fluorescence intensity is seen for the debris (arrows). The field of view in the fluorescent images (**b**) and (**c**) was narrowed by the diaphragm in the fluorescent light path.

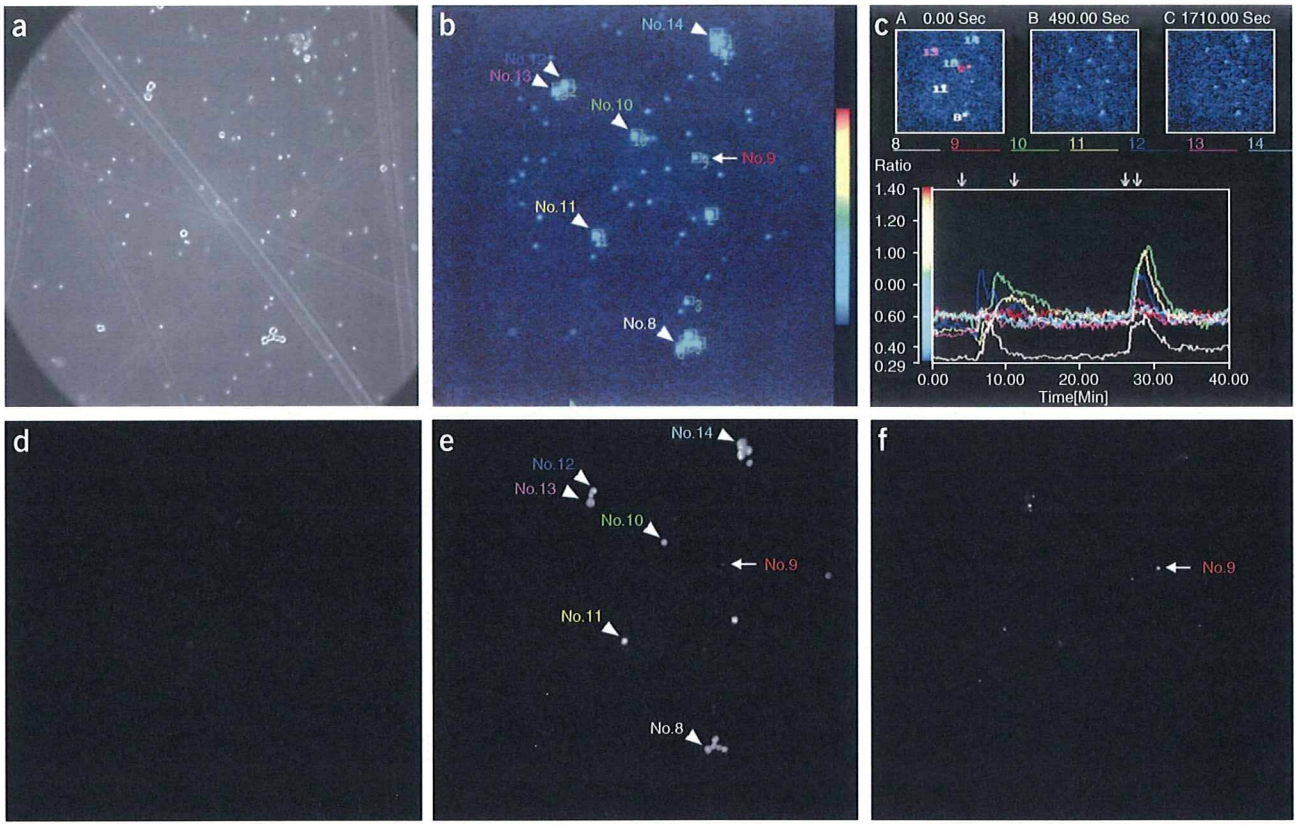

Figure 6 | Measurement of $[Ca^{2+}]_i$ in response to glucose stimulation and subsequent 2-[*N*-(7-nitrobenz-2-oxa-1,3-diazol-4-yl)amino]-2-deoxy-D-glucose (2-NBDG) uptake in living pancreatic islet cells followed by immunocytochemical identification. (**a**) Transmitted light image (×20). Scratches made under the glass bottom of the dish are visible. (**b**) Raw fluorescent image examined at 500–520-nm wavelength for 380-nm excitation after loading of 1 μM fura-2/AM by superfusion. Areas demarcated by squares were tentatively selected for monitoring $[Ca^{2+}]_i$ responses before starting the measurement. Of these, the responses of cells indicated by colored numbers are exemplified (see below). (**c**) A window of the Argus 50 for $[Ca^{2+}]_i$ analysis. Seven areas can be analyzed on one page of the Argus 50 (seven colors are assigned automatically). Areas showing increases (no. 8 and nos. 10–14) and no increase (no. 9) in $[Ca^{2+}]_i$ are expressed as the change in fura-2 fluorescence ratio (340 or 380 nm) (lower panel). Small downward arrows above the lower panel indicate periods of superfusing Krebs Ringer bicarbonate buffer (KRB) containing 16.8 mM glucose (between the two left arrows) and 200 μM tolbutamide (between the right arrows). The response times to tolbutamide coincided for cells responding to high glucose, whereas the response times to glucose varied, indicating inaccuracy of the superfusion and differences in intracellular metabolism after glucose uptake among cells. Upper insets are provided by the software for checking locations of cells and changes in the fluorescence at different time points. Fluorescent images measured at 540-nm wavelength (**d**) before and (**e**) after loading 200 μM 2-NBDG for 1 min. Cells incorporating 2-NBDG are β-cells[9], and uptake of 2-NBDG into cell no. 9 was undetectable during 1 min loading. (**f**) Immunocytochemistry of glucagon. Rhodamine-conjugated secondary antibody was used. Cell no. 9 (arrow) was clearly immunopositive for glucagon. Rhodamine fluorescence was examined with a 590-nm longpass filter (excitation wavelength 510–560 nm). Note that the location of the cells incorporating abundant 2-NBDG can be identified by their vague fluorescence. In (**a**–**e**), cells were superfused continuously with KRB containing 2.8 mM glucose at 37 °C, and the KRB was supplemented as indicated. In these original pictures, no subtraction or shading correction was done. Contrast was adjusted for clarity only in panels (**d**) and (**e**). Note that some cells were lost and some not seen in the original transmitted light image entered from upstream during superfusion. Some of these data were first published in ref. 9.

some investigators use a very low concentration of 2-NBDG (10μM)[13]. For a long loading period, time-dependent extinction should also be considered. In MIN6 cells, the intensity of 2-NBDG fluorescence (200μM loaded for 60 s) was linearly decreased to 87.7, 70.9 and 56.6% 15, 30 and 60 min after uptake, respectively, under dark condition (K. Yamada and N. Inagaki, unpublished data). Care should be taken that the actual loading period of 2-NBDG from the beginning of superfusion to complete washing is constant for all of the cells compared. Differences in the local temperature within the area of interest should be within 1°C (e.g., 36.5–37.5 °C) to minimize temperature-dependent variance of the uptake[8].

? TROUBLESHOOTING

10| When 2-NBDG uptake is evaluated in the presence of glucose, skip Step 8 and change the superfusate to KRB containing 2-NBDG and glucose. The glucose concentration added to the KRB should be determined according to the purpose of experiment. To test inhibition of 2-NBDG uptake by D-glucose, superfuse cells with KRB containing 11.2 mM D-glucose and compare the 2-NBDG uptake with that in the absence of D-glucose. The uptake of 2-NBDG (600μM loaded for 2 min) in the presence of 11.2 mM glucose was significantly inhibited by 52.5 ± 6.3% compared with uptake in the absence of glucose[8].

11| After washing for 5 min, capture fluorescent images.

12| Calculate the relative fluorescence intensity of each cell before and after loading 2-NBDG by subtracting the corresponding background fluorescence from the fluorescence intensity of the cells.

13| Calculate the net increase in the fluorescence intensity for each cell by subtracting the relative fluorescence intensity before from that after loading 2-NBDG.

14| To test whether the 2-NBDG uptake occurs through GLUTs, superfuse cells with KRB containing 10μM cytochalasin B 5 min before the 2-NBDG loading. In MIN6 cells, the increase in fluorescence by loading 200μM 2-NBDG for 15 s was almost completely inhibited in the presence of cytochalasin B[9].

? TROUBLESHOOTING

Troubleshooting advice can be found in **Table 1**.

TABLE 1 | Troubleshooting table.

Step	Problem	Possible reasons	Solution
9	Variable results in 2-[*N*-(7-nitrobenz-2-oxa-1,3-diazol-4-yl)amino]-2-deoxy-D-glucose (2-NBDG) fluorescence in quantitative measurements or high background fluorescence due to 2-NBDG	Unstable superfusion in the chamber	Check for smooth superfusion by dropping a small amount of dye such as pontamine sky blue (Brilliant Blue 6B, CI-24420, Tokyo Chemical Industry, Tokyo, Japan) using an extra dish without cells. Adjust the position of the outlet needle so that it slightly protrudes into the glass bottom part. Adjust the inlet angle and direction finely so that a smooth, laminar flow is obtained. A constant sound of sucking of the superfusate from the outlet needle indicates a stable flow. Measure the temperature of each region of interest with a thin thermistor probe to confirm that the temperature difference is within 1 °C. An area meeting this criterion can be marked on the cover glass. Measurement of the local temperature also helps in finding irregular flow
		Pollution by 2-NBDG fluorescence from the forceps used for placing and removing the plastic plate on the glass-bottom culture dish, or other materials such as the thermistor probe	Every time a dish is exchanged, the plate and forceps used should be rinsed thoroughly. Make several additional plates to save time. Each time vacuum grease is taken from the tube, use a new disposable toothpick so that the grease itself is not polluted by 2-NBDG fluorescence. Similar care should be taken for other parts
		Variance of uptake specific to the particular cell types of interest	See ANTICIPATED RESULTS

ANTICIPATED RESULTS

An example of the raw measurements of 2-NBDG uptake in MIN6 cells is shown in **Figure 5**. The fluorescence of MIN6 cells, which was only slightly discernible before loading, was remarkably increased by a brief (15 s) superfusion of 600μM 2-NBDG in the absence of glucose. In the transmitted light image, cells with an abnormal round shape are easily distinguished from normal cells exhibiting irregular shape[24]. Abnormal cells and areas where multiple cells are overlapping are to be excluded from the

analysis. MIN6 cells exhibit a relatively homogeneous uptake of 2-NBDG. However, when other cell types are used, care should be taken to determine whether the variable uptake of 2-NBDG is due to intrinsic differences in the glucose uptake of individual cells (**Box 2**, **Box 3** and **Fig. 6**).

ACKNOWLEDGMENTS We are grateful to our collaborators, Drs. Masanori Nakata and Naoki Horimoto. We also thank Drs. K. Yoshizaki and S. Sato for technical help, and Dr. J. Miyazaki (Osaka University) for providing us with MIN6 cells.

COMPETING INTERESTS STATEMENT The authors declare no competing financial interests.

Published online at http://www.natureprotocols.com
Reprints and permissions information is available online at http://npg.nature.com/reprintsandpermissions

1. Sokoloff, L. Sites and mechanisms of function-related changes in energy metabolism in the nervous system. *Dev. Neurosci.* **15**, 194–206 (1993).
2. Heimberg, H., De Vos, A., Pipeleers, D., Thorens, B. & Schuit, F. Differences in glucose transporter gene expression between rat pancreatic a- and b-cells are correlated to differences in glucose transport but not in glucose utilization. *J. Biol. Chem.* **270**, 8971–8975 (1995).
3. Sokoloff, L. *et al.* The [^{14}C]deoxyglucose method for the measurement of local cerebral glucose utilization: theory, procedure, and normal values in the conscious and anesthetized albino rat. *J. Neurochem.* **28**, 897–916 (1977).
4. Turkheimer, F. *et al.* The use of spectral analysis to determine regional cerebral glucose utilization with positron emission tomography and [^{18}F]fluorodeoxyglucose: theory, implementation, and optimization procedures. *J. Cereb. Blood Flow Metab.* **14**, 406–422 (1994).
5. Dienel, G.A., Cruz, N.F., Adachi, K., Sokoloff, L. & Holden, J.E. Determination of local brain glucose level with [^{14}C]methylglucose: effects of glucose supply and demand. *Am. J. Physiol.* **273**, E839–E849 (1997).
6. Axelrod, J.D. & Pilch, P.F. Unique cytochalasin B binding characteristics of the hepatic glucose carrier. *Biochemistry* **22**, 2222–2227 (1983).
7. Yoshioka, K. *et al.* A novel fluorescent derivative of glucose applicable to the assessment of glucose uptake activity of *Escherichia coli*. *Biochim. Biophys. Acta* **1289**, 5–9 (1996).
8. Matsuoka, H. *et al.* Viable cell detection by the combined use of fluorescent glucose and fluorescent glycine. *Biosci. Biotechnol. Biochem.* **67**, 2459–2462 (2003).
9. Yamada, K. *et al.* Measurement of glucose uptake and intracellular calcium concentration in single, living pancreatic β-cells. *J. Biol. Chem.* **275**, 22278–22283 (2000).
10. Miyazaki, J. *et al.* Establishment of a pancreatic beta cell line that retains glucose-inducible insulin secretion: special reference to expression of glucose transporter isoforms. *Endocrinology* **127**, 126–132 (1990).
11. Lloyd, P.G., Hardin, C.D. & Sturek, M. Examining glucose transport in single vascular smooth muscle cells with a fluorescent glucose analogue. *Physiol. Res.* **48**, 401–410 (1999).
12. Roman, Y., Alfonso, A., Carmen Louzao, M., Vieytes, M.R. & Botana, L.M. Confocal microscopy study of the different patterns of 2-NBDG uptake in rabbit enterocytes in the apical and basal zone. *Eur. J. Physiol.* **443**, 234–239 (2001).
13. Ball, S.W., Bailey, J.R., Stewart, J.M., Vogels, C.M. & Westcott, S.A. A fluorescent compound for glucose uptake measurements in isolated rat cardiomyocytes. *Can. J. Physiol. Pharmacol.* **80**, 205–209 (2002).
14. Loaiza, A., Porras, O.H. & Barros, L.F. Glutamate triggers rapid glucose transport stimulation in astrocytes as evidenced by real-time confocal microscopy. *J. Neurosci.* **23**, 7337–7342 (2003).
15. Bernardinelli, Y., Magistretti, P.J. & Chatton, J.-Y. Astrocytes generate Na-mediated metabolic waves. *Proc. Natl. Acad. Sci. USA* **101**, 14937–14942 (2004).
16. Porras, O.H., Loaiza, A. & Barros, F. Glutamate mediates acute glucose transport inhibition in hippocampal neurons. *J. Neurosci.* **24**, 9669–9673 (2004).
17. Itoh, Y., Abe, T., Takaoka, R. & Tanahashi, N. Fluorometric determination of glucose utilization in neurons *in vitro* and *in vivo*. *J. Cereb. Blood Metab.* **24**, 993–1003 (2004).
18. Blomstrand, F. & Giaume, C. Kinetics of endothelin-induced inhibition and glucose permeability of astrocyte gap junctions. *J. Neurosci. Res.* **83**, 996–1003 (2006).
19. O'Neil, R.G., Wu, L. & Mullani, N. Uptake of a fluorescent deoxyglucose analogue (2-NBDG) in tumor cells. *Mol. Imaging Biol.* **7**, 388–392 (2005).
20. Cheng, Z. *et al.* Near-infrared fluorescent deoxyglucose analogue for tumor optical imaging in cell culture and living mice. *Bioconjug. Chem.* **17**, 662–669 (2006).
21. Nakata, M. *et al.* Effects of statins on the adipocyte maturation and expression of glucose transporter 4 (SLC2A4): implications in glycaemic control. *Diabetologia* **49**, 1881–1892 (2006).
22. Zou, C., Wang, Y. & Shen, Z. 2-NBDG as a fluorescent indicator for direct glucose uptake measurement. *J. Biochem. Biophys. Methods* **64**, 207–215 (2005).
23. Yoshioka, K. *et al.* Intracellular fate of 2-NBDG, a fluorescent probe for glucose uptake activity, in *Escherichia coli* cells. *Biosci. Biotech. Biochem.* **60**, 1899–1901 (1996).
24. Minami, K. *et al.* Insulin secretion and differential gene expression in glucose-responsive and -unresponsive MIN6 sublines. *Am. J. Physiol. Endocrinol. Metab.* **279**, E773–E781 (2000).
25. Yada, T., Itoh, K. & Nakata, M. Glucagon-like peptide-1-(7-36)amide and a rise in cyclic adenosine 3,5-monophosphate increase cytosolic free Ca^{2+} in rat pancreatic beta-cells by enhancing Ca^{2+} channel activity. *Endocrinology* **133**, 1685–1692 (1993).

Available online at www.sciencedirect.com
ScienceDirect
Biochemical and Biophysical Research Communications 367 (2008) 793–798
BBRC
www.elsevier.com/locate/ybbrc

GLP-1 receptor signaling protects pancreatic beta cells in intraportal islet transplant by inhibiting apoptosis

Kentaro Toyoda [a], Teru Okitsu [b], Shunsuke Yamane [a], Taeko Uonaga [a], Xibao Liu [a], Norio Harada [a], Shinji Uemoto [c], Yutaka Seino [d], Nobuya Inagaki [a,e,*]

[a] *Department of Diabetes and Clinical Nutrition, Graduate School of Medicine, Kyoto University, 54 Kawahara-cho, Shogoin Sakyo-ku, Kyoto 606-8507, Japan*
[b] *Transplantation Unit, Kyoto University Hospital, Kyoto 606-8507, Japan*
[c] *Department of Surgery, Graduate School of Medicine, Kyoto University, Kyoto 606-8507, Japan*
[d] *Kansai Denryoku Hospital, Osaka 553-0003, Japan*
[e] *CREST of Japan Science and Technology Cooperation (JST), Kyoto, Japan*

Received 6 January 2008
Available online 22 January 2008

Abstract

To clarify the cytoprotective effect of glucagon-like peptide-1 receptor (GLP-1R) signaling in conditions of glucose toxicity *in vivo*, we performed murine isogenic islet transplantation with and without exendin-4 treatment. When a suboptimal number of islets (150) were transplanted into streptozotocin-induced diabetic mice, exendin-4 treatment contributed to the restoration of normoglycemia. When 50 islets expressing enhanced green fluorescent protein (EGFP) were transplanted, exendin-4 treatment reversed loss of both the number and mass of islet grafts one and 3 days after transplantation. TUNEL staining revealed that exendin-4 treatment reduced the number of apoptotic beta cells during the early posttransplant phase, indicating that GLP-1R signaling exerts its cytoprotective effect on pancreatic beta cells by inhibiting their apoptosis. This beneficial effect might be used both to ameliorate type 2 diabetes and to improve engraftment rates in clinical islet transplantation.

Keywords: Exendin-4; Glucagon-like peptide-1; Cytoprotection; Apoptosis; Enhanced green fluorescent protein; Islet transplantation; Islet engraftment

Glucagon-like peptide-1 (GLP-1) is a physiological incretin, an intestinal hormone released in response to nutrient ingestion that stimulates glucose-dependent insulin secretion [1,2]. Recent studies have demonstrated that GLP-1 has beneficial effects on pancreatic beta cells [3–6], one of which is inhibition of apoptosis of native beta cells. *In vitro* studies have shown that GLP-1 receptor (GLP-1R) signaling has various beneficial actions such as ameliorating ER stress [7,8] and oxidative stress [9]. However, demonstration of the *in vivo* cytoprotective effect in an animal model of type 2 diabetes (T2DM) is problematic because enhancement of GLP-1R signaling reduces blood glucose levels due to its insulinotropic action [4,5], glucagonostatic action on alpha cells [10], and improvement of insulin sensitivity [11], which makes it difficult to evaluate the cytoprotective effects in the same conditions of glucose toxicity.

To clarify the cytoprotective effect of GLP-1R signaling *in vivo*, we used a murine isogenic islet transplantation model using a suboptimal number of islets together with exendin-4 treatment, a degradation-resistant GLP-1 analog [12]. As isogenic islet grafts in the natural course of the early posttransplant period are easily lost due to various physiological stress [13], various suboptimal number of islet transplantation can lead proper engraftment during the transplantation process without regard for the effects of improved blood glucose levels following transplantation

* Corresponding author. Address: Department of Diabetes and Clinical Nutrition, Graduate School of Medicine, Kyoto University, 54 Kawahara-cho, Shogoin Sakyo-ku, Kyoto 606-8507, Japan. Fax: +81 75 751 4244.
E-mail address: inagaki@metab.kuhp.kyoto-u.ac.jp (N. Inagaki).

0006-291X/$ - see front matter © 2008 Elsevier Inc. All rights reserved.
doi:10.1016/j.bbrc.2008.01.046

of an optimal number of islets. When a higher suboptimal mass of islets is transplanted, blood glucose levels remain high during the early posttransplant period, changing to normoglycemic only during the late posttransplantation period if the engrafted mass is sufficient but remaining in the hyperglycemic state if the engrafted mass is insufficient. Thus, when a suboptimal number of islets are transplanted together with exendin-4 treatment in the early posttransplant period when the recipient is hyperglycemic, its indirect action on glucose tolerance can be excluded and its cytoprotective effect can be evaluated by monitoring the blood glucose levels. In addition, bio-imaging technology permits comparison of the number and mass of islets before and after transplantation.

In the present study, we evaluated the cytoprotective effect of GLP-1R signaling *in vivo* in pancreatic beta cells using a murine isogenic islet transplantation model. We used a suboptimal mass of transplanted islets with and without exendin-4 treatment, and monitored blood glucose levels. We also compared the number and mass of islet grafts with and without exendin-4 treatment under conditions of hyperglycemia.

Materials and methods

Animal care. All experiments were approved by the Kyoto University Animal Care Committee.

Animals. Male C57BL/6JJcl mice (CREA, Japan) aged 8–10 weeks were used as recipients and donors. Male transgenic C57BL/6-EGFP mice aged 8–10 weeks were also used as donors. The mice were obtained from Dr. Masaru Okabe (Research Institute for Microbial Diseases, Osaka University, Osaka, Japan) [14]. Recipient animals were rendered diabetic by a single intraperitoneal injection of streptozotocin (Sigma–Aldrich, USA), 120 mg/kg body weight, freshly dissolved in 10 mM citrate buffer (pH 4.2). Mice with a blood glucose concentration greater than 20 mmol/l for 2 consecutive days were used as recipients. Blood glucose concentrations were determined by glucose meter (Glucocard, Arkley, Japan).

Islet isolation, islet transplantation, and exendin-4 treatment. Islets were isolated, as previously described [15]. Recipient mice were anesthetized by isoflurane (Forane, Abott, Japan). Fresh islets in a volume of 400 μl PBS solution were injected into the portal vein and transplanted into the right hepatic lobe as previously described [15,16]. Exendin-4 at a dosage of 1.0 nmol/kg body weight was administered intraperitoneally once daily in the morning for 14 days.

Oral glucose tolerance test (OGTT). After fasting for 16 h, a basal blood sample was collected and the mice received glucose (1.5 g/kg body weight) orally; additional blood samples were collected at 15, 30, 60, 90, and 120 min after glucose loading.

Evaluation of number and mass of EGFP-expressing islet grafts. Islets isolated from transgenic C57BL/6-EGFP mice were first observed by fluorescence microscope BZ-8000 (KeyEnce, Japan) before transplantation; the area of fluorescence was measured using Image J software (National Institute of Mental Health, USA). Livers bearing islet grafts were removed and sectioned into 500-μm slices and serialized; digitalized photographs of all sections were taken. The number of EGFP-positive islets in each liver section was then counted, excepting those appearing by their position to be part of an islet in an adjacent section. The total area of fluorescence of all islets was then measured.

Measurement of beta-cell mass using immunohistochemistry. The right hepatic lobes were fixed, embedded in paraffin, cut in blocks at regular intervals, and sectioned into 5-μm sections. Deparaffinized sections were incubated with a polyclonal guinea pig anti-insulin antibody (Dako, USA), then with a biotinylated goat anti-guinea pig antibody (Vector, USA), and then with a streptavidin peroxidase conjugate and substrate kit (Dako). The total liver area and total insulin-positive beta-cell area were quantified using Image J software.

Apoptosis detection. TUNEL staining was performed using Apoptosis detection Kit (Takara Bio, Japan).

Statistical analyses. All data are presented as means ± SEM. Statistical analyses were performed by an unpaired *t*-test. p value of less than 0.05 was considered significant.

Results

Exendin-4 decreased the number of islet grafts required to restore normoglycemia

To evaluate the cytoprotective effect of GLP-1R signaling during the early posttransplant phase, we performed isogenic islet transplantation and observed blood glucose levels during the late posttransplant phase. Previous reports have shown that transplantation of only 75 islets can normalize blood glucose levels if the majority becomes engrafted [17], but because many islets are lost due to various stress such as glucotoxicity, transplantation of 75 islets is insufficient for restoration of normoglycemia. In our preliminary experiments, while some recipients showed improved blood glucose levels when 200 islets were transplanted (data not shown), no recipients showed any change in blood glucose levels when 150 islets were transplanted (Fig. 1A). Thus, 150 islets was chosen as an appropriate suboptimal number for use in these transplantation experiments. In addition, all mice transplanted with 150 islets together with exendin-4 treatment became hyperglycemic soon after transplantation but became normoglycemic approximately 14 days after transplantation (Fig. 1A). The responsibility of the islet grafts in exendin-4-treated mice in maintenance of glucose tolerance is demonstrated by the immediate return to hyperglycemia after removal the right hepatic lobe (Fig. 1B). In addition, OGTT was similar in mice receiving 150 islets with exendin-4 treatment and sham-operated control mice (Fig. 1C). These results indicate that exendin-4 treatment played a crucial role in the restoration of normoglycemia by protecting the transplanted islets from damage during the early posttransplant phase.

Detection of fluorescence of transplanted Islets of transgenic C57BL/6-EGFP mice

To clarify the cytoprotective effect of exendin-4 *in vivo*, we established a novel system whereby the total number and the total mass of islets can be compared before and after transplantation by using fluorescent islets isolated from transgenic C57BL/6-EGFP mice. These mice exhibited normal pancreas and islet morphology and well as normal glucose tolerance by OGTT (data not shown).

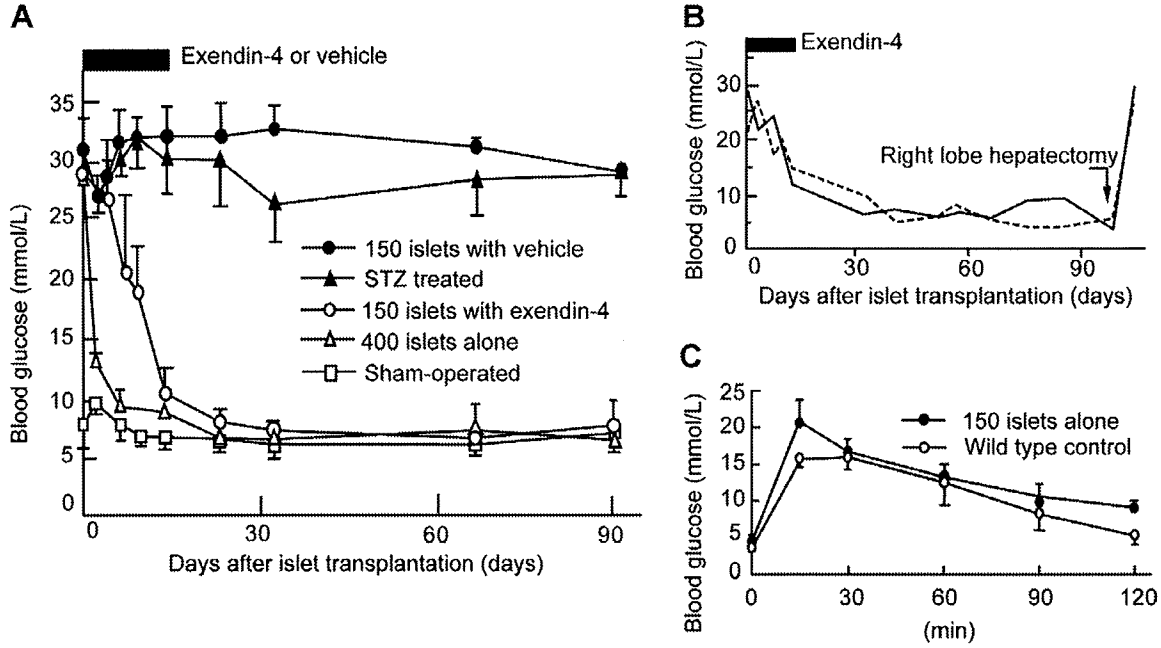

Fig. 1. Exendin-4 reduced the number of islets required for transplantation to restore normoglycemia in STZ-induced diabetic mice. (A) Blood glucose concentrations were measured in mice transplanted with 150 islets together with 1 nmol/kg exendin-4 treatment (open circles, $n = 4$), 400 islets alone (filled triangles, $n = 5$), 150 islets alone (filled circles, $n = 3$), STZ-treated only (filled triangles, $n = 5$), and Sham-operated C57BL/6 mice (open squares, $n = 5$). (B) Right hepatic lobe was resected from two recipients transplanted with 150 islets together with exendin-4 treatment on Day 90 to clarify the effect of the islet grafts on glycemic control. (C) OGTT was performed on Day 30 in recipients transplanted with 150 islets together with exendin-4 treatment and in sham-operated wild-type C57BL/6 mice ($n = 3$ for each).

Transplanted islets of transgenic C57BL/6-EGFP mice are traceable and measurable in both number and mass

To confirm traceability and measurability of the transplanted islets, intraportal transplantation of islets isolated from transgenic C57BL/6-EGFP mice was performed. One day and three days after transplantation, the right hepatic lobe was resected and sliced, and each slice was photographed by fluorescence microscope (Fig. 2A–C). Liver slices containing islet grafts were then immunostained for insulin. The area of fluorescence (Fig. 2A) coincided with that of the islet beta cells stained for insulin (Fig. 2B), demonstrating traceability of the islets. The number of islet grafts in the liver after transplantation was then compared. When 25, 50, or 75 islets were transplanted, the total number of islet grafts detected in the liver was 24.3 ± 0.3, 48.7 ± 0.8 and 73.3 ± 0.3, respectively ($n = 3$ for each), demonstrating a significant ($p < 0.0001$), strong correlation ($r = 1.000$) between the number of detected islet grafts in the liver and the number of transplanted islets (Fig. 2E). In addition, because the area of fluorescence coincided with that of immunostained islets (Fig. 2A–C), the total area of fluorescence reflected the total area mass of the islets, allowing comparison of total islet mass before and after transplantation. When 25, 50, and 75 islets were transplanted, the total area mass of islets before transplantation was 2.01 ± 0.04, 4.11 ± 0.01, and 5.89 ± 0.09 (mm^2), respectively, while that of islet grafts in the liver were 2.00 ± 0.02, 4.28 ± 0.07, and 6.08 ± 0.03 (mm^2), respectively ($n = 3$ for each), demonstrating a significant ($p < 0.0001$), strong ($r = 0.998$) correlation between before and after transplantation (Fig. 2F).

Exendin-4 reduced loss of transplanted islets from transgenic C57BL/6-EGFP mice during the early posttransplant phase

To exclude the indirect effect of exendin-4 through its effect on blood glucose levels, we reduced the number of the transplanted islets to 50. When 50 islets of transgenic C57BL/6-EGFP mice were transplanted with or without treatment of exendin-4 into STZ-induced diabetic mice, the blood glucose levels were not significantly different on 1 day (Day 1) ($n = 3$, 27.1 ± 0.3 vs 27.8 ± 0.1 (mmol/l), $p = 0.193$) or 3 days (Day 3) after transplantation ($n = 3$, 28.7 ± 0.2 vs 28.7 ± 0.3 (mmol/l), $p = 0.936$). The number and the total area mass of the islet grafts in livers resected on Day 1 (figure not shown) and Day 3 (Fig. 3A and B) were then examined. The number of islet grafts with treatment of exendin-4 (Ex(+)) showed 9.4% and 19.9% increases on Day 1 ($n = 3$ for each, 46.7 ± 0.51 vs 42.0 ± 0.33, $p < 0.05$) and Day 3 ($n = 3$ for each, 44.6 ± 0.36 vs 34.7 ± 0.84, $p < 0.01$) (Fig. 3C) compared to those without treatment (Ex(−)). Ex(+) islet grafts exhibited 29.0% and 31.9% more total area mass on Day 1 ($n = 3$ for each, $69.5 \pm 2.5\%$ vs $53.3 \pm 2.1\%$ (normalized to the total fluorescence area mass before transplantation), $p < 0.05$) and Day 3 ($n = 3$ for each, $64.5 \pm 2.6\%$ vs $26.9 \pm 1.1\%$, $p < 0.05$) (Fig. 3D), respectively, than Ex(−).

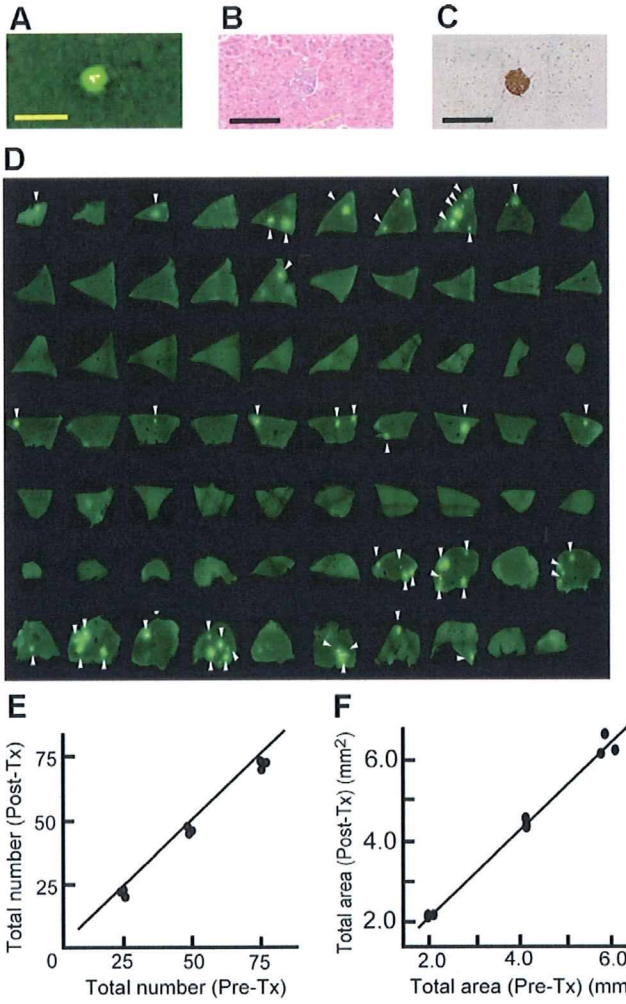

Fig. 2. Islets of transgenic C57BL/6-EGFP mice detected and measured by fluorescence microscopy. (A–C) Photographs of islet grafts in liver. Fluorescent islet (A), HE (B) and insulin immunostaining (C). Scale bar: 200 μm. (D) Representative photographs after transplantation with 50 islets of liver slices under fluorescence microscope. Fluorescent islets are indicated by arrowhead. (E, F) The total number (E) and the total area mass (F) of all EGFP-expressing islets before transplantation compared with fluorescent islet grafts in liver after transplantation ($n = 3$).

Area of islet grafts in liver with and without exendin-4 treatment compared by conventional immunohistochemical analysis

Conventional total area mass measurements, the ratio of the area of islet beta cells to that of the examined liver slice, was compared by immunohistochemical analysis using limited liver sections on Day 1 and Day 3 (Fig. 4A(a and c) and B (e and g)). The conventional relative area mass in Ex(+) was 32.0% and 44.7% higher on Day 1 ($n = 3$ for each, $0.07830 \pm 0.0003\%$ vs $0.0533 \pm 0.0003\%$, $p < 0.05$) and Day 3 ($n = 3$ for each, $0.0680 \pm 0.0009\%$ vs $0.0380 \pm 0.0043\%$, $p < 0.01$) than Ex(−) (Fig. 4C). The ratio of conventional relative area mass of Ex(+) to that of Ex(−) on Day 1 and Day 3 was comparable to the results of measurement of total area mass measured by our novel method.

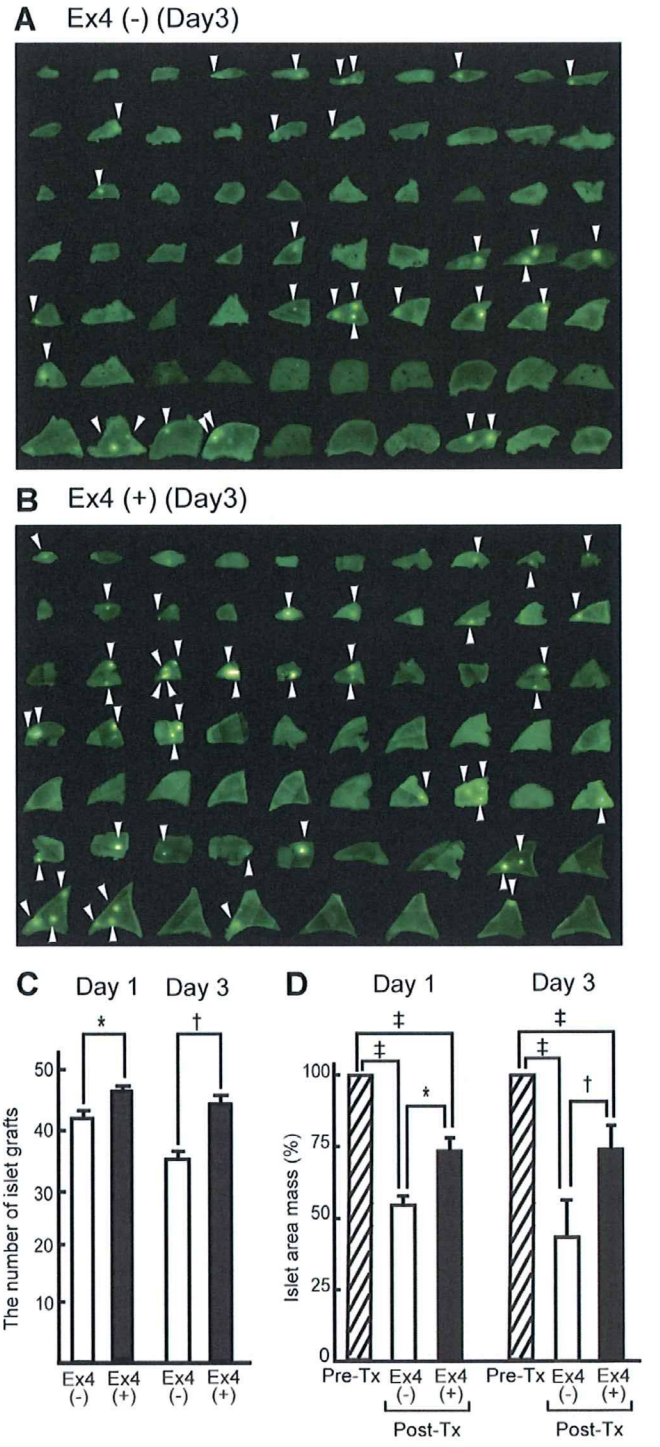

Fig. 3. Exendin-4 preserved transplanted islets during the early posttransplant period in number and total area mass. (A–B) Representative photographs of fluorescent islet grafts in all liver slices from exendin-4-treated mice (Ex4(+)) (A) and -untreated mice (Ex4(−)) (B) on Day 3. (C) Number of islet grafts in liver slices on Day 1 ($n = 3$) and Day 3 ($n = 3$) in Ex4(+) and Ex4(−). $^{*}p < 0.05$ and $^{\dagger}p < 0.01$ vs Ex4(−). (D) Total area mass of all fluorescent islet grafts in liver slices on Day 1 ($n = 3$) and on Day 3 ($n = 3$) in Ex4(+) and Ex(−). Data after transplantation (Post-Tx) and before transplantation (Pre-Tx) are also compared. $^{*}p < 0.05$ and $^{\dagger}p < 0.01$ vs Ex4(−), $^{\ddagger}p < 0.01$ vs Pre-Tx.

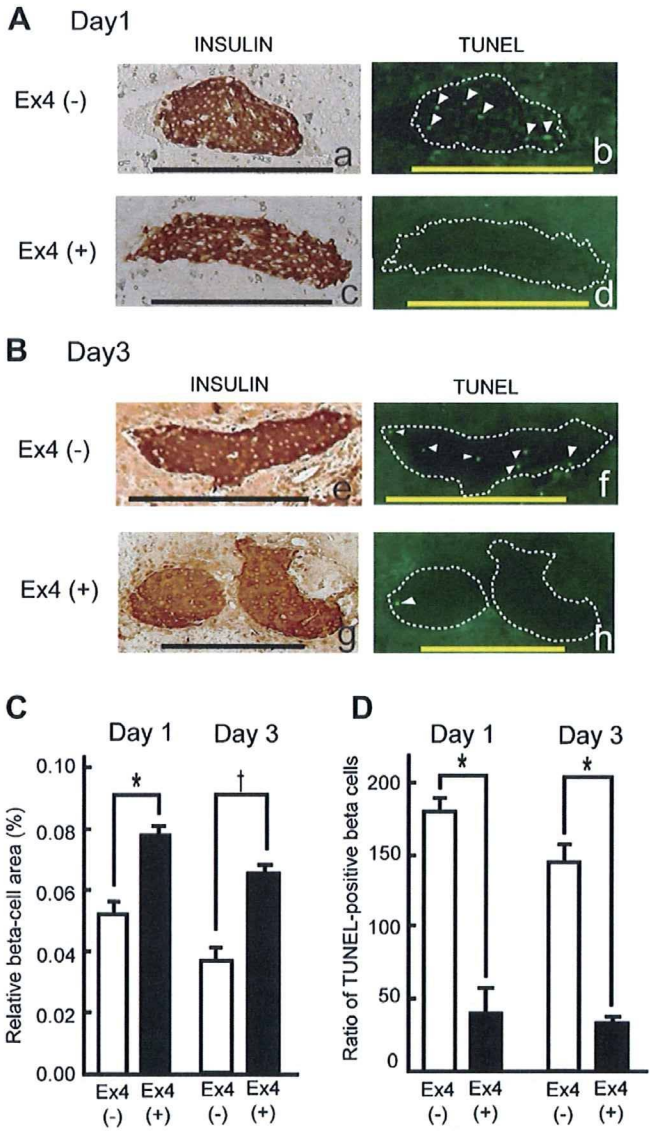

Fig. 4. Exendin-4 treatment reduced beta-cell apoptosis after intraportal islet transplantation. (A–B) Representative photographs of liver sections on Day 1 (A) and Day 3 (B) from Ex4(+) mice and Ex4(−) mice stained for insulin (a, c, e, and g) and TUNEL-assay (b, d, f, and h) are shown. TUNEL-positive cells are indicated by arrowhead. Scale bar: 200 μm. (C) Ex4(+) showed significantly greater beta-cell mass than Ex4(−) on Day 1 ($n = 3$ for each) and Day 3 ($n = 3$ for each). $^{*}p < 0.05$ and $^{\dagger}p < 0.01$ vs Ex4(−). (D) Ex4(+) showed a significantly greater decrease in the ratio of TUNEL-positive beta cells than Ex4(−) on Day 1 ($n = 3$ for each) (number/beta-cell area (mm^2)) and Day 3 ($n = 3$ for each) (number/beta-cell area (mm^2)). $^{*}p < 0.05$ vs Ex4(−).

Exendin-4 decreased the rate of apoptosis of beta cells introduced by intraportal islet graft after transplantation

To investigate the difference in area mass of transplanted islets in Ex(+) and Ex(−), the rate of apoptosis of beta cells of islet grafts on Day 1 and Day 3 was examined (Fig. 4A and B). The rate of apoptosis of TUNEL and insulin-double positive cells was significantly lower on Day 1 ($n = 3$ for each, 246.5 ± 5.5 vs 36.4 ± 3.6 (number/beta-cell area (mm^2), $p < 0.01$) and on Day 3 ($n = 3$ for each, 148.7 ± 17.7 vs 41.3 ± 1.3 (number/beta-cell area (mm^2), $p < 0.01$) with Ex(+) than Ex(−) (Fig. 4D).

Discussion

In the present study, we demonstrate that GLP-1R signaling has a cytoprotective effect in the posttransplant period using a murine islet transplantation model. Exendin-4 treatment during the early posttransplant hyperglycemic phase contributed to restore normoglycemia during the late posttransplant phase in STZ-induced diabetic mice receiving a suboptimal graft of 150 islets. In addition, the total number and total area mass of the islet grafts both on Day 1 and Day 3 was significantly greater in Ex(+) than in Ex(−). The finding that the rate of apoptosis was less in Ex(+) than in Ex(−) both on Day 1 and Day 3, when their blood glucose levels were yet unchanged, demonstrates that GLP-1R signaling inhibits apoptosis *in vivo* under conditions of glucose toxicity.

Murine islet transplantation is an ideal model for investigating the cytoprotective effect of exendin-4 on transplanted pancreatic beta cells *in vivo*. Although isogenic islets injected into the portal vein are spared rejection by the immune reaction, the cells may succumb to apoptosis due to various stress factors including hypoxia [18,19], inflammation [20,21], and mechanical shear stress [22,21] before engraftment. The efficacy of exendin-4 treatment on posttransplant hyperglycemic status in this transplantation model can be quantified using different suboptimal numbers of islets because the posttransplant glycemic condition directly reflects the mass of engrafted islets. The number and mass of transplanted islets can be traced because isolated islets can be labeled and examined before transplantation. Thus, this murine islet transplantation model allows observation of the direct effect of the cytoprotective effect on beta cells *in vivo*.

In this study, we established a method for tracing the transplanted islets of transgenic C57BL/6-EGFP mice in liver sections under fluorescence excitation. Our findings reveal that the area of fluorescence of islet grafts in liver coincides with that of insulin immunostaining (Fig. 2A–C), which areas before transplantation correlate highly with those after transplantation (Fig. 2F). Observation of each islet grafts before and after transplantation is definitive for evaluation of the cytoprotective action, which is not practicable by the conventional immunohistochemical method due to the necessarily limited observation of the organ.

We have also shown that the natural course of islet engraftment in the early posttransplant period can involve loss of about half of the transplanted beta cells. Recently, Eich et al. reported evaluation of islet mass by positron-emission tomography using islets labeled with ^{18}Fluorodeoxyglucose, and found that almost 50% of the transplanted islets in the graft were lost [23], which is comparable with our data. Although about 30% of the graft was found to be lost even with exendin-4 treatment on Day 1, the rate

of apoptosis remained lower, resulting in a mass of engraftment more than adequate for normoglycemia thereafter. This finding is encouraging regarding the possible clinical use of exendin-4 in islet transplantation therapy in human subjects [24,25].

Although exendin-4 is already in clinical use for treatment of T2DM [26], this cytoprotective effect on beta cells *in vivo* also certainly functions independently of other actions in T2DM. The mass of islets is usually already decreased when patients are diagnosed with T2DM [27]. Thus, exendin-4 treatment used in the early phase of development, when glycemic tolerance is yet normal, might hamper the progression of T2DM.

Acknowledgments

This work was supported in part by a Scientific Grant and a Grant-in-Aid for Exploratory Research from the Ministry of Education, Culture, Sports, Science, and Technology of Japan, and by Research on Nanotechnical Medicine from the Ministry of Health, Labour, and Welfare of Japan. We thank Dr. M. Okabe for providing us transgenic C57BL/6-EGFP mice.

References

[1] H. Elrick, L. Stimmler, C.J. Hlad Jr., Y. Arai, Plasma insulin response to oral and intravenous glucose administration, J. Clin. Endocrinol. Metab. 24 (1964) 1076–1082.

[2] M.J. Perley, D.M. Kipnis, Plasma insulin responses to oral and intravenous glucose: studies in normal and diabetic subjects, J. Clin. Invest. 46 (1967) 1954–1962.

[3] Y. Li, T. Hansotia, B. Yusta, F. Ris, P.A. Halban, D.J. Drucker, Glucagon-like peptide-1 receptor signaling modulates beta cell apoptosis, J. Biol. Chem. 278 (2003) 471–478.

[4] P.L. Brubaker, D.J. Drucker, Minireview: Glucagon-like peptides regulate cell proliferation and apoptosis in the pancreas, gut, and central nervous system, Endocrinology 145 (2004) 2653–2659.

[5] J.F. List, J.F. Habener, Glucagon-like peptide 1 agonists and the development and growth of pancreatic beta-cells, Am. J. Physiol. Endocrinol. Metab. 286 (2004) E875–E881.

[6] D.J. Drucker, The biology of incretin hormones, Cell Metab. 3 (2006) 153–165.

[7] B. Yusta, L.L. Baggio, J.L. Estall, J.A. Koehler, D.P. Holland, H. Li, D. Pipeleers, Z. Ling, D.J. Drucker, GLP-1 receptor activation improves beta cell function and survival following induction of endoplasmic reticulum stress, Cell Metab. 4 (2006) 391–406.

[8] J. Sun, H. He, B.J. Xie, Novel antioxidant peptides from fermented mushroom Ganoderma lucidum, J. Agric. Food Chem. 52 (2004) 6646–6652.

[9] H. Wang, G. Kouri, C.B. Wollheim, ER stress and SREBP-1 activation are implicated in beta-cell glucolipotoxicity, J. Cell Sci. 118 (2005) 3905–3915.

[10] L.A. Scrocchi, T.J. Brown, N. MaClusky, P.L. Brubaker, A.B. Auerbach, A.L. Joyner, D.J. Drucker, Glucose intolerance but normal satiety in mice with a null mutation in the glucagon-like peptide 1 receptor gene, Nat. Med. 2 (1996) 1254–1258.

[11] A.A. Young, B.R. Gedulin, S. Bhavsar, N. Bodkin, C. Jodka, B. Hansen, M. Denaro, Glucose-lowering and insulin-sensitizing actions of exendin-4: studies in obese diabetic (ob/ob, db/db) mice, diabetic fatty Zucker rats, and diabetic rhesus monkeys (*Macaca mulatta*), Diabetes 48 (1999) 1026–1034.

[12] L. Hansen, C.F. Deacon, C. Orskov, J.J. Holst, Glucagon-like peptide-1-(7–36)amide is transformed to glucagon-like peptide-1-(9–36)amide by dipeptidyl peptidase IV in the capillaries supplying the L cells of the porcine intestine, Endocrinology 140 (1999) 5356–5363.

[13] J.A. Emamaullee, A.M. Shapiro, Factors influencing the loss of beta-cell mass in islet transplantation, Cell Transplant. 16 (2007) 1–8.

[14] M. Okabe, M. Ikawa, K. Kominami, T. Nakanishi, Y. Nishimune, 'Green mice' as a source of ubiquitous green cells, FEBS Lett. 407 (1997) 313–319.

[15] T. Okitsu, S.T. Bartlett, G.A. Hadley, C.B. Drachenberg, A.C. Farney, Recurrent autoimmunity accelerates destruction of minor and major histoincompatible islet grafts in nonobese diabetic (NOD) mice, Am. J. Transplant. 1 (2001) 138–145.

[16] Y. Yonekawa, T. Okitsu, K. Wake, Y. Iwanaga, H. Noguchi, H. Nagata, X. Liu, N. Kobayashi, S. Matsumoto, A new mouse model for intraportal islet transplantation with limited hepatic lobe as a graft site, Transplantation 82 (2006) 712–715.

[17] A. King, J. Lock, G. Xu, S. Bonner-Weir, G.C. Weir, Islet transplantation outcomes in mice are better with fresh islets and exendin-4 treatment, Diabetologia 48 (2005) 2074–2079.

[18] G. Miao, R.P. Ostrowski, J. Mace, J. Hough, A. Hopper, R. Peverini, R. Chinnock, J. Zhang, E. Hathout, Dynamic production of hypoxia-inducible factor-1alpha in early transplanted islets, Am. J. Transplant. 6 (2006) 2636–2643.

[19] M. Giuliani, W. Moritz, E. Bodmer, D. Dindo, P. Kugelmeier, R. Lehmann, M. Gassmann, P. Groscurth, M. Weber, Central necrosis in isolated hypoxic human pancreatic islets: evidence for postisolation ischemia, Cell Transplant. 14 (2005) 67–76.

[20] N.R. Barshes, S. Wyllie, J.A. Goss, Inflammation-mediated dysfunction and apoptosis in pancreatic islet transplantation: implications for intrahepatic grafts, J. Leukoc. Biol. 77 (2005) 587–597.

[21] S. Cabric, J. Sanchez, T. Lundgren, A. Foss, M. Felldin, R. Kallen, K. Salmela, A. Tibell, G. Tufveson, R. Larsson, O. Korsgren, B. Nilsson, Islet surface heparinization prevents the instant blood-mediated inflammatory reaction in islet transplantation, Diabetes 56 (2007) 2008–2015.

[22] J.L. Contreras, C. Eckstein, C.A. Smyth, G. Bilbao, M. Vilatoba, S.E. Ringland, C. Young, J.A. Thompson, J.A. Fernandez, J.H. Griffin, D.E. Eckhoff, Activated protein C preserves functional islet mass after intraportal transplantation: a novel link between endothelial cell activation, thrombosis, inflammation, and islet cell death, Diabetes 53 (2004) 2804–2814.

[23] T. Eich, O. Eriksson, T. Lundgren, Visualization of early engraftment in clinical islet transplantation by positron-emission tomography, N. Engl. J. Med. 356 (2007) 2754–2755.

[24] E.A. Ryan, B.W. Paty, P.A. Senior, D. Bigam, E. Alfadhli, N.M. Kneteman, J.R. Lakey, A.M. Shapiro, Five-year follow-up after clinical islet transplantation, Diabetes 54 (2005) 2060–2069.

[25] K.A. Ghofaili, M. Fung, Z. Ao, M. Meloche, R.J. Shapiro, G.L. Warnock, D. Elahi, G.S. Meneilly, D.M. Thompson, Effect of exenatide on beta cell function after islet transplantation in type 1 diabetes, Transplantation 83 (2007) 24–28.

[26] D.M. Kendall, M.C. Riddle, J. Rosenstock, D. Zhuang, D.D. Kim, M.S. Fineman, A.D. Baron, Effects of exenatide (exendin-4) on glycemic control over 30 weeks in patients with type 2 diabetes treated with metformin and a sulfonylurea, Diabetes Care 28 (2005) 1083–1091.

[27] A.E. Butler, J. Janson, S. Bonner-Weir, R. Ritzel, R.A. Rizza, P.C. Butler, Beta-cell deficit and increased beta-cell apoptosis in humans with type 2 diabetes, Diabetes 52 (2003) 102–110.

Biochemical and Biophysical Research Communications 376 (2008) 21–25

Contents lists available at ScienceDirect

Biochemical and Biophysical Research Communications

journal homepage: www.elsevier.com/locate/ybbrc

Inhibition of GIP signaling modulates adiponectin levels under high-fat diet in mice

Rei Naitoh [a], Kazumasa Miyawaki [a], Norio Harada [a], Wataru Mizunoya [b], Kentaro Toyoda [a], Tohru Fushiki [b], Yuichiro Yamada [a,c], Yutaka Seino [a,d], Nobuya Inagaki [a,e,*]

[a] Department of Diabetes and Clinical Nutrition, Graduate School of Medicine, Kyoto University, 54 Shogoin Kawahara-cho, Sakyo-ku, Kyoto 606-8507, Japan
[b] Division of Food Science and Biotechnology, Graduate School of Agriculture, Kyoto University, Kyoto, Japan
[c] Department of Endocrinology and Diabetes and Geriatric Medicine, Akita University School of Medicine, Akita, Japan
[d] Kansai Electric Power Hospital, Osaka, Japan
[e] CREST of Japan Science and Technology Cooperation (JST), Kyoto, Japan

ARTICLE INFO

Article history:
Received 8 August 2008
Available online 22 August 2008

Keywords:
GIP
Fat oxidation
Adiponectin
PPAR

ABSTRACT

Gastric inhibitory polypeptide (GIP) is an incretin and directly promotes fat accumulation in adipocytes. Inhibition of GIP signaling prevents onset of obesity and increases fat oxidation in peripheral tissues under high-fat diet (HFD), but the mechanism is unknown. In the present study, we investigated the effects of inhibition of GIP signaling on adiponectin levels after 3 weeks of HFD by comparing wild-type (WT) mice and GIP receptor-deficient ($Gipr^{-/-}$) mice. In HFD-fed $Gipr^{-/-}$ mice, fat oxidation was significantly increased and adiponectin mRNA levels in white adipose tissue and plasma adiponectin levels were significantly increased compared to those in HFD-fed WT mice. In addition, the PPARα mRNA level was increased and the ACC mRNA level was decreased in skeletal muscle of HFD-fed $Gipr^{-/-}$ mice compared with those in HFD-fed WT mice. These results indicate that inhibition of GIP signaling increases adiponectin levels, resulting in increased fat oxidation in peripheral tissues under HFD.

Gastric inhibitory polypeptide (GIP) is a major incretin that potentiates insulin secretion in pancreatic β-cells in the presence of glucose [1,2]. GIP is released from duodenal endocrine K-cells after meal ingestion, and acts by binding the GIP receptor through increased intracellular cAMP [3]. The GIP receptor is expressed in pancreas, stomach, small intestine, heart, adrenal cortex, brain, lung, bone, vascular endothelium, and adipose tissue [4]. In addition to the insulinotropic effects on pancreatic β-cells, GIP is an obesity-promoting factor that directly leads to the accumulation of fat in adipocytes. In vitro studies show that GIP stimulates synthesis and secretion of lipoprotein lipase (LPL) in cultured preadiocytes [5], and that GIP promotes LPL activity in fat tissue [6]. It also has been shown that GIP stimulates glucose transport and increases fatty-acid synthesis in fat tissue [7]. Studies of GIP receptor-deficient mice ($Gipr^{-/-}$ mice) show that GIP also is an important factor in the promotion of obesity in vivo [8]. High-fat diet (HFD)-fed wild-type (WT) mice exhibit body weight gain and markedly increased visceral and subcutaneous fat mass and liver steatosis. By contrast, $Gipr^{-/-}$ mice fed HFD exhibit neither weight gain nor adiposity. Furthermore, measurement of the respiratory quotient reveals that fat is used as the preferred energy substrate in $Gipr^{-/-}$ mice. In addition, a study using IRS-$1^{-/-}$/$Gipr^{-/-}$ double-deficient mice demonstrated that inhibition of GIP signaling increases fatty-acid oxidation in peripheral tissues under diminished insulin signaling [9]. Thus, GIP plays a critical role in adiposity, but the mechanism of fat oxidation in peripheral tissues in the absence of GIP signaling is unclear.

Adiponectin is one of the major adipokines secreted from adipocytes, and stimulates fat oxidation in peripheral tissues. Adiponectin promotes AMPK activation and PPARα expression and stimulates fat oxidation in skeletal muscle and liver [10]. In the present study, we investigated the effects of the inhibition of GIP signaling on adiponectin levels and the stimulation of fat oxidation that averts obesity by comparing WT mice and $Gipr^{-/-}$ mice fed HFD. To clarify the early response to HFD-induced obesity, we performed the experiments on mice at 3 weeks of HFD and control-fat diet (CD).

Materials and methods

Animals. The generation of $Gipr^{-/-}$ mice (C57BL/6 background) has been described previously [11]. At 7 weeks of age, WT and $Gipr^{-/-}$ mice were fed HFD or CD for 7 weeks. HFD supplied 45% of calories as fat, 35% as carbohydrate, and 20% as protein, with energy density of 3.57 kcal/g. CD supplied 13% of calories as fat, 60% as carbohydrate, and 27% as protein, with energy density of

* Corresponding author. Address: Department of Diabetes and Clinical Nutrition, Graduate School of Medicine, Kyoto University, 54 Shogoin Kawahara-cho, Sakyo-ku, Kyoto 606-8507, Japan. Fax: +81 75 751 4244.
E-mail address: inagki@metab.kuhp.kyoto-u.ac.jp (N. Inagaki).

0006-291X/$ - see front matter © 2008 Elsevier Inc. All rights reserved.
doi:10.1016/j.bbrc.2008.08.052

3.57 kcal/g. Animal care and procedures were approved by the Animal Care Committee of Kyoto University.

Energy expenditure. Energy expenditure was evaluated by measuring respiratory quotient and oxygen consumption by indirect calorimetry every 13 min for 24 h in mice under the fed condition, as described previously [8,9,12]. Air from the room was pumped through the chamber, and expired gas was dried in a cotton thin column and subjected to gas analysis (Alco System model RL-600, Chiba, Japan). O_2 and CO_2 concentrations were measured, and oxygen consumption (VO_2), carbon dioxide exhaustion (VCO_2), respiratory quotient (RQ), and fat oxidation were calculated as described previously [12].

Computed tomography. Mice were anesthetized with pentobarbital and fixed in a chamber, and transaxially scanned using Latheta (LCT-100M) experimental animal CT system (Aloka, Tokyo, Japan). The whole body was scanned, and contiguous 1-mm slice images of the trunk were used for quantitative assessment (Latheta software, version 1.00). Weight of visceral fat mass and lean mass were quantitatively evaluated.

Measurement of plasma adiponectin levels and Western blot analysis. Blood samples were collected from the tail vein at the end of the dark phase and centrifuged (3000 rpm, 10 min, 4 °C). Levels of plasma adiponectin were measured using an adiponectin ELISA kit (Otsuka, Tokyo, Japan).

Plasma samples of HFD-fed mice were subjected to SDS–PAGE using Laemmli's method [13]. SDS–PAGE was performed under non-reducing and non-heat-denaturing conditions, as previously reported [14]. Western blot analysis was performed using anti-mouse adiponectin antibody. Densities of corresponding bands were quantified by NIH-Image.

Isolation of total RNA and quantitative RT-PCR. Total RNA was isolated from muscle and white adipose tissue (epididymal fat pad, (WAT)) using Trizol (Invitrogen, Grand Island, NY). mRNA levels were measured by real-time quantitative RT-PCR using ABI PRISM 7000 Sequence Detection System (Applied Biosystems, Foster City, CA). mRNA levels were corrected for GAPDH (Applied Biosystems) mRNA level. Sequences of PPARα primers were 5′-CGACCTGAAAG ATTCGGAAA-3′ and 5′-CCTCTGCCTCTTTGTCTTC-3′; sequences of ACC primers were 5′-CCTCCGAGGAACCCTCTGT-3′ and 5′-CGGCTGT CCAGTTGGTTTG-3′; sequences of adiponectin primers were 5′-G GAACTTGTGCAGGTTGGAT-3′ and 5′-GCTTCTCCAGGCTCTCCTTT-3′; and sequences of PPARγ primers were 5′-TGTCGGTTTCAGAAGT GCCTT-3′ and 5′-GCTCGCAGATCAGCAGACTCT-3′.

Statistical analysis. Data are expressed as means ± SE. Statistical analysis was performed by ANOVA and unpaired student's test. *P* values <0.05 were considered significant.

Results

Body weight and fat mass in HFD-fed Gipr$^{-/-}$ mice

WT mice exhibited significant weight gain after 3 weeks of HFD feeding (Fig. 1A). By contrast, body weight of HFD-fed Gipr$^{-/-}$ mice was not increased compared with that of CD-fed Gipr$^{-/-}$ mice after 3 weeks of study (Fig. 1B). The lesser body weight of Gipr$^{-/-}$ mice continued through 7 weeks of HFD feeding.

At the early stage of 3 weeks of HFD feeding, CT analysis was performed to estimate visceral fat mass in WT and Gipr$^{-/-}$ mice. There was no significant difference in visceral fat mass between WT and Gipr$^{-/-}$ mice under CD feeding. Visceral fat mass of HFD-fed WT and Gipr$^{-/-}$ mice were significantly increased compared with those of CD-fed WT and Gipr$^{-/-}$ mice by 100% and 52%, respectively. In HFD-fed mice, visceral fat mass of WT mice was significantly increased compared with that of Gipr$^{-/-}$ mice (Fig. 1C and D). There was no difference in lean body mass (data not shown). There also was no difference in food intake between WT and Gipr$^{-/-}$ mice (data not shown).

Fat consumption in HFD-fed Gipr$^{-/-}$ mice

To evaluate energy consumption in the early stage of HFD feeding, respiratory quotient and oxygen consumption were measured

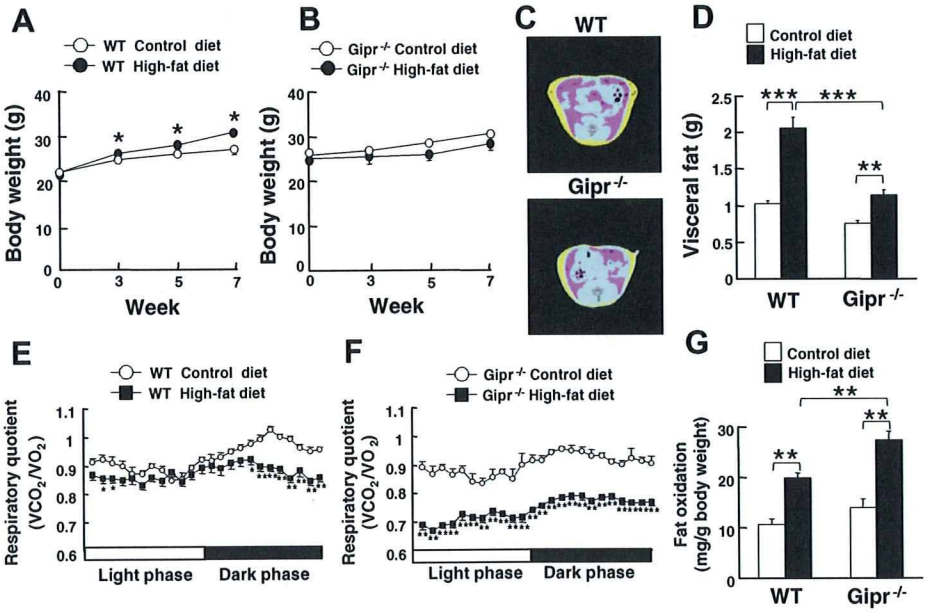

Fig. 1. Body weight in WT mice (A) and Gipr$^{-/-}$ mice (B) during 7 weeks on CD (open circles) and HFD (filled circles). (C) CT-based body composition analysis. WT mice and Gipr$^{-/-}$ mice at 3 weeks on HFD feeding. Representative CT images were taken at the same slice level. Pink, yellow, and blue areas represent visceral fat, subcutaneous fat, and lean mass. (D) Visceral fat accumulation in WT mice and Gipr$^{-/-}$ mice at 3 weeks on CD (open bars) and HFD (filled bars). Respiratory quotient in WT mice (E) and Gipr$^{-/-}$ mice (F) at 3 weeks on CD (open circles) and HFD (filled square). (G) Calculated fat oxidation in WT mice and Gipr$^{-/-}$ mice at 3 weeks on CD (open bars) and HFD (filled bars). n = 5–12. Values are means ± SE. $^{*}P < 0.05$, $^{**}P < 0.01$, $^{***}P < 0.005$. (For interpretation of the references to color in this figure legend, the reader is referred to the web version of this paper.)

by indirect calorimetry. HFD-fed WT mice exhibited a significant reduction of respiratory quotient only in part of the dark phase compared with CD-fed WT mice (Fig. 1E). By contrast, HFD-fed Gipr$^{-/-}$ mice exhibited a significant reduction of respiratory quotient throughout the day compared with CD-fed Gipr$^{-/-}$ mice (Fig. 1F). At 3 weeks of HFD feeding, calculated fat oxidation was significantly increased in Gipr$^{-/-}$ mice compared with that in WT mice (Fig. 1G). These results indicate that Gipr$^{-/-}$ mice use fat as preferred energy substrate in the early stage of HFD feeding.

Adiponectin levels of Gipr$^{-/-}$ mice in the early stage of HFD feeding

We examined mRNA expression level of adiponectin in white adipose tissue (WAT) and plasma adiponectin levels in Gipr$^{-/-}$ mice. mRNA expression of adiponectin in WAT and plasma adiponectin levels were significantly increased in HFD-fed Gipr$^{-/-}$ mice compared with those in HFD-fed WT mice (Fig. 2A and B). In addition, in Gipr$^{-/-}$ mice, mRNA expression level of adiponectin in WAT and plasma adiponectin levels were significantly increased in HFD-fed mice compared with those in CD-fed mice, although HFD feeding decreased mRNA expression of adiponectin and plasma adiponectin levels in WT mice (Fig. 2A and B).

To determine qualitative differences in adiponectin, we performed Western blot analysis. Levels of middle molecular weight (MMW) and low molecular weight (LMW) multimers of adiponectin were significantly higher in HFD-fed Gipr$^{-/-}$ mice compared to those in HFD-fed WT mice (Fig. 2C and Table 1). There were no significant differences in high molecular weight multimers (HMW) of adiponectin between HFD-fed WT and Gipr$^{-/-}$ mice.

As PPARγ (peroxisome proliferator-activated receptor-γ) is known to be involved in the regulation of adiponectin, we examined mRNA expression levels of PPARγ in WAT. While HFD-fed WT mice showed a tendency to decreased mRNA expression of PPARγ, the mRNA expression level of PPARγ was significantly increased in HFD-fed Gipr$^{-/-}$ mice compared with that in HFD-fed WT mice (Fig. 2D). These results suggest that inhibition of GIP signaling modulates adiponectin levels through PPARγ.

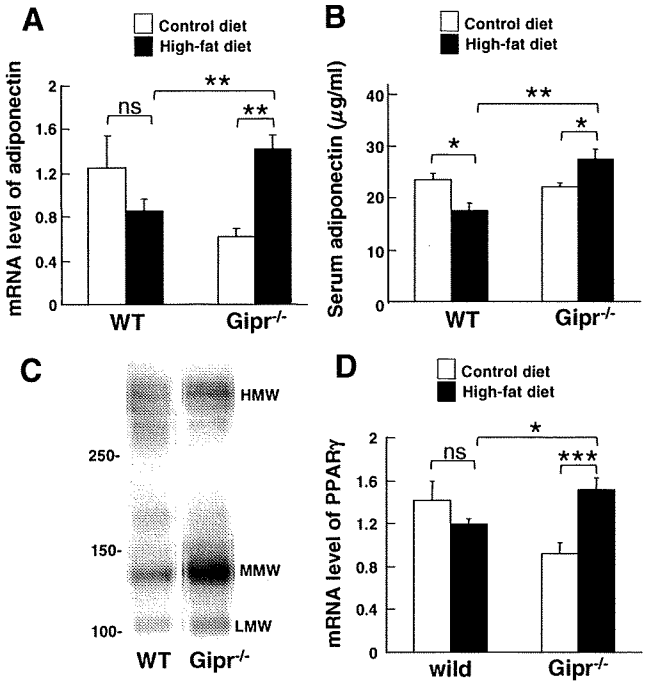

Fig. 2. mRNA expression level of adiponectin in WAT (A) and plasma adiponectin level (B) at 3 weeks on CD (open bars) and HFD (filled bars). $n = 7$–8 mice/group. Values are means ± SE. $^{*}P < 0.05$, $^{**}P < 0.01$. (C) Non-reducing and non-heat-denaturing SDS–PAGE of adiponectin in WT mice and Gipr$^{-/-}$ mice at 3 weeks on HFD. (D) mRNA expression level of PPARγ in WAT at 3 weeks on CD (open bars) and HFD (filled bars). $n = 4$–7. Values are means ± SE. $^{*}P < 0.05$, $^{***}P < 0.005$. ns, not significant.

Table 1
Difference in multimer formation of adiponectin in WT mice and Gipr$^{-/-}$ mice at 3 weeks on high-fat diet

	WT	Gipr$^{-/-}$
HMW	100 ± 22.0	131.9 ± 17.8
MMW	100 ± 9.1	154.3 ± 5.9*
LMW	100 ± 13	163.4 ± 15.3*

Values for Gipr$^{-/-}$ mice represent relative density (%) regarding average value for WT mice as 100. $n = 5$. Values are means ± SE.
* $P < 0.05$ vs. WT mice.

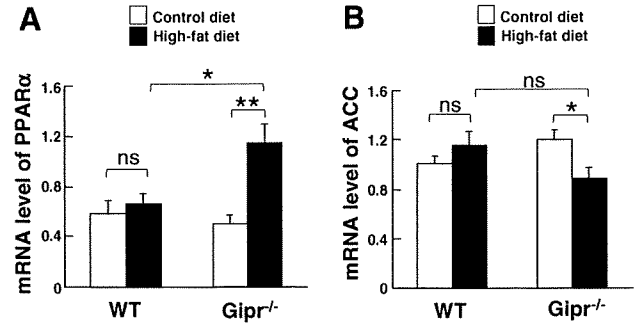

Fig. 3. mRNA expression level of PPARα (A) and ACC (B) in skeletal muscle at 3 weeks on CD (open bars) and HFD (filled bars). $n = 5$–7. Values are means ± SE. $^{*}P < 0.05$, $^{**}P < 0.01$. ns, not significant.

Expression levels of PPARα and ACC mRNAs in skeletal muscle of Gipr$^{-/-}$ mice at the early stage of HFD feeding

To determine the effects of adiponectin on peripheral tissues in the absence of GIP signaling, mRNA expression levels of PPARα (peroxisome proliferator-activated receptor-α) and ACC (acetyl-CoA carboxylase) in skeletal muscle and liver were examined. mRNA expression level of PPARα mRNA was significantly increased in HFD-fed Gipr$^{-/-}$ mice compared with that in CD-fed Gipr$^{-/-}$ mice in skeletal muscle (Fig. 3A). Although there was no significant difference in phosphorylation of AMPK (AMP-activated protein kinase) between HFD-fed WT and Gipr$^{-/-}$ mice by western blot analysis (data not shown), mRNA expression level of ACC, which is inactivated by AMPK, was significantly reduced in muscle of HFD-fed Gipr$^{-/-}$ mice compared with that in CD-fed Gipr$^{-/-}$ mice (Fig. 3B). These results indicate that fat oxidation is increased in skeletal muscle of Gipr$^{-/-}$ mice in the early stage of HFD feeding. We also examined mRNA expression levels of PPARα and ACC in liver, but no significant differences were found among the groups of mice (data not shown).

Discussion

In this study, we investigated the effects of GIP inhibition on fat oxidation in the early stage (3 weeks) of HFD feeding, and found that inhibition of GIP signaling increases the level of adiponectin, which promotes fat oxidation in peripheral tissues.

The GIP receptor is expressed in adipocytes as well as in pancreatic β-cells, and GIP signaling directly promotes energy accumulation into adipocytes. Previously, Gipr$^{-/-}$ mice were shown to exhibit resistance to high-fat-induced obesity, and to use fat as the preferred energy substrate [8]. In that study, mice were fed

HFD for a long period of from 7 to 50 weeks of age. In the present study, we investigated HFD-fed mice in the short, early period from 7 to 10 weeks of age, and found Gipr$^{-/-}$ mice to be resistant to obesity as well as to accumulation of visceral fat, and that fat oxidation was significantly increased, demonstrating that GIP plays a critical role in promoting obesity even at 3 weeks on HFD feeding.

Leptin and adiponectin are major adipokines that activate fat oxidation for body weight control. They affect AMPK activation and stimulate fat oxidation in skeletal muscle and liver [10,15]. It has been reported that inhibition of GIP signaling decreases body weight even in leptin-deficient ob/ob mice [8], indicating that factors other than leptin increase fat oxidation under conditions of inhibited GIP signaling. Leptin suppresses food intake through the central nervous system, and there were no differences in food intake between WT and Gipr$^{-/-}$ mice in CD-fed and HFD-fed mice in the present study. Thus, we focused on adiponectin, and hypothesized that inhibition of GIP signaling modulates adiponectin levels and affects on fat oxidation in peripheral tissues. The mRNA expression level of adiponectin in adipocytes and adiponectin concentrations in plasma are reduced in obese and insulin-resistant states which increases visceral fat mass [16,17]. In the present study, mRNA expression level of adiponectin in WAT and plasma adiponectin levels were found to be decreased and visceral fat mass was increased in HFD-fed WT mice compared with CD-fed WT mice. The mRNA expression and plasma levels of adiponectin were significantly increased in HFD-fed Gipr$^{-/-}$ mice compared with those in CD-fed Gipr$^{-/-}$ mice, although visceral fat mass of HFD-fed Gipr$^{-/-}$ mice was significantly increased compared with that of CD-fed Gipr$^{-/-}$ mice. These results suggest that GIP may reduce adiponectin levels in adipocytes. It has been previously reported that Gipr$^{-/-}$ mice show no difference in plasma adiponectin levels between CD-fed and HFD-fed mice after a long period of 20 weeks, when obesity is established [18]. On the other hand, we measured adiponectin levels of mice fed HFD for a short period of 3 weeks, and demonstrate that inhibition GIP signaling modulates adiponectin even in the very early stage when obesity first begins to appear in WT mice.

While skeletal muscle and liver are the major sites of body fat oxidation, the GIP receptor is not expressed in these tissues. PPARα and AMPK are the most important molecules in the control of fat oxidation in muscle and liver. Adiponectin increases expression levels of PPARα and induces phosphorylation of AMPK [16,19]. AMPK activated by adiponectin suppresses ACC activity, which catalyses the formation of malonyl-CoA and stimulates fat oxidation [20]. We found that the mRNA expression level of PPARα was significantly increased and that of ACC was significantly reduced in skeletal muscle of HFD-fed Gipr$^{-/-}$ mice compared to those in CD-fed Gipr$^{-/-}$ mice. These results indicate that fat oxidation is increased in skeletal muscle of Gipr$^{-/-}$ mice in the early stage of HFD feeding, but there was no significant difference in liver. Adiponectin has three forms: trimers (low molecular weight, LMW), hexamers (middle molecular weight, MMW), and multimers (high molecular weight, HMW), and differing tissue-specific effects of these forms on AMPK phosphorylation have been reported [21]. Only trimers activate AMPK in muscle; hexamers and the high molecular isoform do not [22]. It also has been reported that trimers are the most potent isoform in skeletal muscle [19,23]. The trimer isoform of adiponectin was found in the present study to be significantly increased in HFD-fed Gipr$^{-/-}$ mice. This finding may explain the difference of PPARα and ACC expression between skeletal muscle and liver in HFD-fed Gipr$^{-/-}$ mice.

In conclusion, we show that inhibition of GIP signaling upregulates the adiponectin level and increases fat oxidation in skeletal muscle. These findings suggest that the influence of GIP on adiposity is, at least in part, mediated by modulation of adiponectin expression in adipocytes in the early stage of HFD feeding.

Acknowledgments

We thank Drs. Takashi Kadowaki and Naoto Kubota (Department of Diabetes and Metabolic Disease, Tokyo University Graduate School of Medicine) for providing anti-mouse adiponectin antibody and for their valuable suggestion.

We also thank Drs. Katsushi Tsukiyama, Rie Watanabe, Heying Zhou, Chizumi Yamada, and Yukiko Kawasaki for their technical help and for their valuable comments.

This study was supported by Scientific Research Grants from the Ministry of Education, Culture, Sports, Science, and Technology, Japan, and from the Ministry of Health, Labor, and Welfare, Japan.

References

[1] P. Schauder, J. Brown, H. Frerichs, W. Creutzfeldt, Gastric inhibitory polypeptide: effect on glucose-induced insulin release from isolated rat pancreatic islets in vitro, Diabetologia 11 (1975) 483–484.
[2] J. Dupre, S. Ross, D. Watson, J. Brown, Stimulation of insulin secretion by gastric inhibitory polypeptide in man, J. Clin. Endocrinol. Metab. 37 (1973) 826–828.
[3] Y. Yamada, K. Miyawaki, K. Tsukiyama, N. Harada, C. Yamada, Y. Seino, Pancreatic and extrapancreatic effects of gastric inhibitory polypeptide, Diabetes 55 (Suppl. 2) (2006) S86–S91.
[4] T.B. Usdin, E. Mezey, D.C. Button, M.J. Brownstein, T.I. Bonner, Gastric inhibitory polypeptide receptor, a member of the secretin-vasoactive intestinal peptide receptor family, is widely distributed in peripheral organs and the brain, Endocrinology 133 (1993) 2861–2870.
[5] R.H. Eckel, W.Y. Fujimoto, J.D. Brunzell, Gastric inhibitory polypeptide enhanced lipoprotein lipase activity in cultured preadipocytes, Diabetes 28 (1979) 1141–1142.
[6] J. Knapper, S. Puddicombe, L. Morgan, J. Fletcher, Investigations into the actions of glucose-dependent insulinotropic polypeptide and glucagon-like peptide-1(7-36)amide on lipoprotein lipase activity in explants of rat adipose tissue, J. Nutr. 125 (1995) 183–188.
[7] H. Hauner, G. Glatting, D. Kaminska, E. Pfeiffer, Effects of gastric inhibitory polypeptide on glucose and lipid metabolism of isolated rat adipocytes, Ann. Nutr. Metab. 32 (1988) 282–288.
[8] K. Miyawaki, Y. Yamada, N. Ban, Y. Ihara, K. Tsukiyama, H. Zhou, S. Fujimoto, A. Oku, K. Tsuda, S. Toyokuni, H. Hiai, W. Mizunoya, T. Fushiki, J. Holst, M. Makino, A. Tashita, Y. Kobara, Y. Tsubamoto, T. Jinnouchi, T. Jomori, Y. Seino, Inhibition of gastric inhibitory polypeptide signaling prevents obesity, Nat. Med. 8 (2002) 738–742.
[9] H. Zhou, Y. Yamada, K. Tsukiyama, K. Miyawaki, M. Hosokawa, K. Nagashima, K. Toyoda, R. Naitoh, W. Mizunoya, T. Fushiki, T. Kadowaki, Y. Seino, Gastric inhibitory polypeptide modulates adiposity and fat oxidation under diminished insulin action, Biochem. Biophys. Res. Commun. 335 (2005) 937–942.
[10] T. Kadowaki, T. Yamauchi, Adiponectin and adiponectin receptors, Endocr. Rev. 26 (2005) 439–451.
[11] K. Miyawaki, Y. Yamada, H. Yano, H. Niwa, N. Ban, Y. Ihara, A. Kubota, S. Fujimoto, M. Kajikawa, A. Kuroe, K. Tsuda, H. Hashimoto, T. Yamashita, T. Jomori, F. Tashiro, J. Miyazaki, Y. Seino, Glucose intolerance caused by a defect in the entero-insular axis: a study in gastric inhibitory polypeptide receptor knockout mice, Proc. Natl. Acad. Sci. USA 96 (1999) 14843–14847.
[12] K. Ishihara, S. Oyaizu, K. Onuki, K. Lim, T. Fushiki, Chronic (−)-hydroxycitrate administration spares carbohydrate utilization and promotes lipid oxidation during exercise in mice, J. Nutr. 130 (2000) 2990–2995.
[13] U.K. Laemmli, Cleavage of structural proteins during the assembly of the head of bacteriophage T4, Nature 227 (1970) 680–685.
[14] H. Waki, T. Yamauchi, J. Kamon, Y. Ito, S. Uchida, S. Kita, K. Hara, Y. Hada, F. Vasseur, P. Froguel, S. Kimura, R. Nagai, T. Kadowaki, Impaired multimerization of human adiponectin mutants associated with diabetes. Molecular structure and multimer formation of adiponectin, J. Biol. Chem. 278 (2003) 40352–40363.
[15] Y. Minokoshi, Y. Kim, O. Peroni, L. Fryer, C. Müller, D. Carling, B. Kahn, Leptin stimulates fatty-acid oxidation by activating AMP-activated protein kinase, Nature 415 (2002) 339–343.
[16] T. Yamauchi, J. Kamon, H. Waki, Y. Imai, N. Shimozawa, K. Hioki, S. Uchida, Y. Ito, K. Takakuwa, J. Matsui, M. Takata, K. Eto, Y. Terauchi, K. Komeda, M. Tsunoda, K. Murakami, Y. Ohnishi, T. Naitoh, K. Yamamura, Y. Ueyama, P. Froguel, S. Kimura, R. Nagai, T. Kadowaki, Globular adiponectin protected ob/ob mice from diabetes and ApoE-deficient mice from atherosclerosis, J. Biol. Chem. 278 (2003) 2461–2468.
[17] C. Weyer, T. Funahashi, S. Tanaka, K. Hotta, Y. Matsuzawa, R. Pratley, P. Tataranni, Hypoadiponectinemia in obesity and type 2 diabetes: close association with insulin resistance and hyperinsulinemia, J. Clin. Endocrinol. Metab. 86 (2001) 1930–1935.
[18] T. Hansotia, A. Maida, G. Flock, Y. Yamada, K. Tsukiyama, Y. Seino, D.J. Drucker, Extrapancreatic incretin receptors modulate glucose homeostasis, body weight, and energy expenditure, J Clin Invest 117 (2007) 143–152.
[19] T. Yamauchi, J. Kamon, H. Waki, Y. Terauchi, N. Kubota, K. Hara, Y. Mori, T. Ide, K. Murakami, N. Tsuboyama-Kasaoka, O. Ezaki, Y. Akanuma, O. Gavrilova, C.

Vinson, M. Reitman, H. Kagechika, K. Shudo, M. Yoda, Y. Nakano, K. Tobe, R. Nagai, S. Kimura, M. Tomita, P. Froguel, T. Kadowaki, The fat-derived hormone adiponectin reverses insulin resistance associated with both lipoatrophy and obesity, Nat. Med. 7 (2001) 941–946.
[20] B. Kiens, Skeletal muscle lipid metabolism in exercise and insulin resistance, Physiol. Rev. 86 (2006) 205–243.
[21] M. Barnea, A. Shamay, A. Stark, Z. Madar, A high-fat diet has a tissue-specific effect on adiponectin and related enzyme expression, Obesity (Silver Spring) 14 (2006) 2145–2153.
[22] T. Tsao, E. Tomas, H. Murrey, C. Hug, D. Lee, N. Ruderman, J. Heuser, H. Lodish, Role of disulfide bonds in Acrp30/adiponectin structure and signaling specificity. Different oligomers activate different signal transduction pathways, J. Biol. Chem. 278 (2003) 50810–50817.
[23] J. Fruebis, T. Tsao, S. Javorschi, D. Ebbets-Reed, M. Erickson, F. Yen, B. Bihain, H. Lodish, Proteolytic cleavage product of 30-kDa adipocyte complement-related protein increases fatty acid oxidation in muscle and causes weight loss in mice, Proc. Natl. Acad. Sci. USA 98 (2001) 2005–2010.

Am J Physiol Endocrinol Metab 294: E61–E68, 2008.
First published October 30, 2007; doi:10.1152/ajpendo.00358.2007.

A novel GIP receptor splice variant influences GIP sensitivity of pancreatic β-cells in obese mice

Norio Harada,[1] Yuichiro Yamada,[1] Katsushi Tsukiyama,[1] Chizumi Yamada,[1] Yasuhiko Nakamura,[1] Eri Mukai,[1,2] Akihiro Hamasaki,[1] Xibao Liu,[1] Kentaro Toyoda,[1] Yutaka Seino,[1,3] and Nobuya Inagaki[1,4]

[1]*Department of Diabetes and Clinical Nutrition, Kyoto University Graduate School of Medicine, Kyoto;* [2]*Japan Association for the Advancement of Medical Equipment, Tokyo;* [3]*Kansai Electric Power Hospital, Osaka; and* [4]*Core Research for Evolutional Science and Technology of Japan Science and Technology, Kyoto, Japan*

Submitted 11 June 2007; accepted in final form 11 October 2007

Harada N, Yamada Y, Tsukiyama K, Yamada C, Nakamura Y, Mukai E, Hamasaki A, Liu X, Toyoda K, Seino Y, Inagaki N. A novel GIP receptor splice variant influences GIP sensitivity of pancreatic β-cells in obese mice. *Am J Physiol Endocrinol Metab* 294: E61–E68, 2008. First published October 30, 2007; doi:10.1152/ajpendo.00358.2007.— Gastric inhibitory polypeptide (GIP) is an incretin that potentiates insulin secretion from pancreatic β-cells by binding to GIP receptor (GIPR) and subsequently increasing the level of intracellular adenosine 3′,5′-cyclic monophosphate (cAMP). We have identified a novel GIPR splice variant in mouse β-cells that retains intron 8, resulting in a COOH-terminal truncated form (truncated GIPR). This isoform was coexpressed with full-length GIPR (wild-type GIPR) in normal GIPR-expressing tissues. In an experiment using cells transfected with both GIPRs, truncated GIPR did not lead to cAMP production induced by GIP but inhibited GIP-induced cAMP production through wild-type GIPR ($n = 3$–4, $P < 0.05$). Wild-type GIPR was normally located on the cell surface, but its expression was decreased in the presence of truncated GIPR, suggesting a dominant negative effect of truncated GIPR against wild-type GIPR. The functional relevance of truncated GIPR in vivo was investigated. In high-fat diet-fed obese mice (HFD mice), blood glucose levels were maintained by compensatory increased insulin secretion ($n = 8$, $P < 0.05$), and cAMP production ($n = 6$, $P < 0.01$) and insulin secretion ($n = 10$, $P < 0.05$) induced by GIP were significantly increased in isolated islets, suggesting hypersensitivity of the GIPR. Total GIPR mRNA expression was not increased in the islets of HFD mice, but the expression ratio of truncated GIPR to total GIPR was reduced by 32% compared with that of control mice ($n = 6$, $P < 0.05$). These results indicate that a relative reduction of truncated GIPR expression may be involved in hypersensitivity of GIPR and hyperinsulinemia in diet-induced obese mice.

gastric inhibitory polypeptide; gastric inhibitory polypeptide receptor; alternative splicing; dominant negative effect; obesity

OBESITY LEADS TO INSULIN RESISTANCE, characterized by fasting hyperinsulinemia and excessive insulin secretion after meal ingestion in the attempt to maintain euglycemia (25). Obesity is an important risk factor in progression to type 2 diabetes mellitus (14) and also in cardiovascular disease (16), and reduction of obesity can normalize hyperinsulinemia and impede the progression of diabetes and arteriosclerosis.

Incretins are a group of peptide hormones released from the gastrointestinal tract into the circulation in response to meal ingestion that potentiate glucose-stimulated insulin secretion and include gastric inhibitory polypeptide (GIP), also called glucose-dependent insulinotropic polypeptide (24). GIP is secreted from the K cells of the duodenum and proximal jejunum upon meal ingestion and binds to the GIP receptor (GIPR) on the surface of pancreatic β-cells, adipose tissues, and osteoblasts to stimulate insulin secretion (21), fat accumulation (20), and bone formation (30) by increasing the level of intracellular adenosine 3′,5′-cyclic monophosphate (cAMP).

Previously, we found that GIPR-deficient mice exhibit insufficient compensatory insulin secretion upon high-fat loading (21), indicating that GIP plays a critical role in maintaining the blood glucose level by inducing hypersecretion of insulin in diet-induced obesity. Increased GIP signaling in obesity might be due to hypersecretion of GIP from K cells or hypersensitivity of GIPR to GIP at the β-cells. An increased blood GIP level in obesity has been reported in some studies (3, 6) but is controversial (27, 28), and altered GIPR sensitivity in obesity has not been investigated.

GIPR is the G protein-coupled receptor (GPCR) that belongs to the secretin-vasoactive intestinal peptide receptor family (31, 33). The gene encoding the human GIPR contains 14 exons (33); the rat and mouse GIPR-encoding genes contain 15 exons (2, 21). Alternative splicing is a frequent occurrence in the transcriptome in higher eukaryotic cells and can alter the structure of the encoded protein and dramatically increase the efficiency of the proteome in regulating cell function. In the present study, we report a novel splice variant GIPR expressed in mouse pancreatic β-cells and the investigation of its functional significance in hypersensitivity of GIPR in high-fat diet-induced obese mice.

MATERIALS AND METHODS

Animals. Male C57BL/6 mice (7 wk old) were obtained from Shimizu (Kyoto, Japan). The animals were fed control fat chow (CFD; 10% fat, 20% protein, and 70% carbohydrate by energy) or high-fat chow (HFD; 45% fat, 20% protein, and 35% carbohydrate by energy) for 10 wk. The energy density of both diets was 3.57 kcal/g. After a 16-h fast, oral glucose tolerance tests (OGTTs) (2 g/kg body wt) were performed in CFD and HFD mice. Blood glucose and plasma insulin levels were measured in samples taken at the indicated times. Blood glucose levels were determined by the glucose oxidase method. Plasma insulin levels were determined using enzyme immunoassay (Shibayagi, Gumma, Japan). Animal care and procedures were approved by the Animal Care Committee of Kyoto University.

Address for reprint requests and other correspondence: Y. Yamada, Dept. of Internal Medicine, Div. of Endocrinology, Diabetes, and Geriatric Medicine, Akita University School of Medicine, 1-1-1, Hondo, Akita 010-8543, Japan (e-mail: yamada@gipc.akita-u.ac.jp).

The costs of publication of this article were defrayed in part by the payment of page charges. The article must therefore be hereby marked "*advertisement*" in accordance with 18 U.S.C. Section 1734 solely to indicate this fact.